Available online at www.sciencedirect.com
SCIENCE DIRECT®
Journal of Photochemistry and Photobiology C: Photochemistry Reviews
5 (2004) 79–104
Journal of Photochemistry and Photobiology C: Photochemistry Reviews
www.elsevier.com/locate/jphotochemrev

Review

Intermolecular and supramolecular photoinduced electron transfer processes of fullerene–porphyrin/phthalocyanine systems

Mohamed E. El-Khouly [a,1], Osamu Ito [a,*], Phillip M. Smith [b], Francis D'Souza [b,2]

[a] *Institute of Multidisciplinary Research for Advanced Materials, Tohoku University, Katahira, Aoba-ku, Sendai 980-8577, Japan*
[b] *Department of Chemistry, Wichita State University, 1845 Fairmount, Wichita, KS 67260-0051, USA*

Received 17 November 2003; received in revised form 28 January 2004; accepted 28 January 2004

Abstract

The attainment of a better understanding of the dependence of photoinduced electron transfer reaction rates on the molecular structures of the donor and acceptor entities results in improving the capture and storage of solar energy. Here, the intermolecular and supramolecular electron transfer processes from electron donors (porphyrins (P), chlorophylls (Chl), phthalocyanines (Pc) and naphthalocyanines (Nc)) and their metal derivatives to electron acceptors (fullerenes such as C_{60} and C_{70}) studied by nanosecond and picosecond laser flash photolysis techniques in polar and nonpolar solvents are reviewed. For intermolecular systems in polar solvents, photoinduced electron transfer takes place via the excited triplet states of C_{60}/C_{70} or via the excited triplet states of P/Pc/Nc, yielding solvated radical ions in polar solvents; thus, the back electron transfer rates are generally slow. In the case of the supramolecular dyads and triads formed by axial coordination, hydrogen bonding, crown ether complexation, or rotaxane formation, the photoinduced charge separation takes place mainly from the excited singlet state of the donor; however, the back electron transfer rates are generally quite fast. The relations between structures and photochemical reactivities of these novel supramolecular systems are discussed in relation to the efficiency of charge separation and charge recombination.

Keywords: Porphyrins; Phthalocyanines; Fullerenes; Photoinduced electron transfer; Charge separation; Charge recombination; Self-assembly; Supramolecules; Intermolecular interactions

Contents

* Corresponding author.
E-mail addresses: francis.dsouza@wichita.edu, ito@tagen.tohoku.ac.jp (O. Ito).
[1] Present address: Department of Chemistry, Faculty of Education, Kafr El-Sheikh, Tanta University, Tanta, Egypt.
[2] Co-corresponding author.

1389-5567/$ 20.00
doi:10.1016/j.jphotochemrev.2004.01.003

1. Introduction

The process of photoinduced electron transfer (PET) is of great importance in chemistry and biology [1–15]. One of the most important goals of chemistry during the past century has been the construction and development of molecular and supramolecular-based artificial solar energy harvesting systems that have the ability to absorb light from the sun and convert it to useful and storable forms. One way to store solar energy is in the form of chemical energy, as plants do efficiently during photosynthesis. However, for building efficient artificial solar energy converting systems for this purpose, there are certain requirements that must be met: (i) the light must be captured by antenna molecules and/or sensitizers, leading to "excited states;" (ii) the absorption of the light must result in transfer of an electron to the acceptor entity; (iii) the electron transfer must be directional; and (iv) the lifetimes of the excited states must be long enough for electron transfer to take place. Constructing chemical systems possessing the characteristics listed above has been a very challenging goal for chemists over the past two decades.

Intermolecular PET is a simple process in which an electron is transferred from an electron-donating species (D) to an electron-accepting species (A), producing the radical cation of the donor ($D^{\bullet+}$) and the radical anion of the acceptor ($A^{\bullet-}$), when one of these species is photoexcited [2,15]. If these charged species are utilized as electrons and holes to drive electrical current or promote chemical reactions before back electron transfer leading to the initial states of the reactants occurs (Fig. 1), the light energy is effectively converted into electrical or chemical energy.

A critical factor in PET lies in the successful matching of D and A with suitable electrochemical and photophysical properties for the occurrence of such an exothermic ET [2,15,16,17]. Knowledge of the excited state energies of the chromophores and the redox potentials of D and A is thus an essential requirement for investigating PET processes. The majority of research on the photochemistry of porphyrins is an attempt to mimic the photosynthetic processes, in which

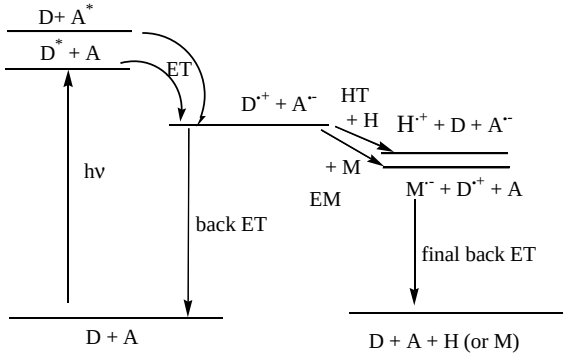

Fig. 1. Schematic energy diagrams for photoinduced ET processes in bimolecular donor–acceptor systems: HT refers to hole transfer step in the presence of hole acceptor (H) and EM refers to an electron mediation step in the presence of an electron mediator (M).

porphyrins have been widely employed as sensitizers and as electron donors [18–20]. As electron-acceptors, benzoquinones and methyl viologens have been used to generate photocurrent and hydrogen evolution [21–23]. Covalently connected porphyrin–quinone dyads and triads have been synthesized to realize long lifetimes of the charge separated states [24–31].

Since the fullerenes were discovered and preparation methods were developed, fullerenes have been utilized as photosensitizers and electron acceptors [32,33]. Fullerenes (C_{60}/C_{70}) exhibit a number of characteristic electronic and photophysical properties, which make them promising candidates for the investigation of PET processes. Some of these characteristics are [32–39]: (i) fullerenes have first reduction potentials comparable to that of benzoquinone [40,41]. Since fullerenes can reversibly accept up to six electrons in electrochemical measurements, and in principle can act as electron accumulators [40,41], there are possibilities to realize a multiple photoreduction process. (ii) In terms of transient absorption spectral features, the singlet excited states of fullerenes (C_{60} and C_{70}) give rise to characteristic singlet–singlet absorptions in the visible and near-IR region [32,33,42–44]. Once generated, the excited singlet states (1.65–1.75 eV) are subject to a rapid and quantitative intersystem crossing process, with a lifetime of 0.9–1.3 ns, to the energetically low lying triplet excited states (1.45–1.55 eV) with lifetimes longer than 40 μs [32,33,44]. (iii) The triplet–triplet absorption spectrum of C_{60} shows a maximum in the visible region (740 nm; $\varepsilon = 18{,}000\,M^{-1}\,cm^{-1}$) [40]; in the case of C_{70}, the triplet–triplet absorption spectrum appears at 980 nm, with $\varepsilon = 4000\,M^{-1}\,cm^{-1}$ [45]. (iv) A more practical aspect of C_{60} and C_{70} concerns the optical absorption spectra of their π-radical anions, such as $C_{60}^{\bullet-}$ and $C_{70}^{\bullet-}$, which show narrow bands in the near-IR region, around 1080 and 1380 nm, respectively, serving as diagnostic probes for their identification [32,33,45–47]. Furthermore, these isolated absorptions allow an accurate analysis of inter- and intramolecular ET dynamics of C_{60} and C_{70}, even in the presence of porphyrins and phthalocyanines, which have wide absorptions in the visible region. For this purpose, it is very important to develop techniques to measure the transient absorption spectra in the near-IR region [50,51]. (v) Fullerene-based electron donor–acceptor dyads exhibit relatively rapid photoinduced charge-separation (CS) and relatively slow charge-recombination (CR) due to the low reorganization energy of fullerenes [48–52]. Achieving a long-lived CS state after photoexcitation is the key to realizing artificial photosynthesis in supramolecular systems.

Porphyrins form a ubiquitous class of naturally occurring molecules. The UV-Vis absorption spectrum of the highly conjugated porphyrin macrocycle exhibits an intense feature (extinction coefficient > 200,000) at about 400 nm (the Soret band) followed by several weaker absorptions (Q bands) at higher wavelengths (from 450 to 750 nm), which are changed by the peripheral substituents on the porphyrin

ring and insertion of metal atoms into the center of the porphyrin ring. The extensively conjugated π-systems of porphyrins increase their electron-donor abilities, so that they are suitable for efficient ET in the ground and excited states. The electronic excited states of porphyrins survive long enough in the singlet and triplet states to provide a high probability to interact with molecules before deactivation [53–58]. Porphyrins are involved in a wide variety of important biological processes, ranging from oxygen transport to photosynthesis [4,53–58]. The role of porphyrins in photosynthetic mechanisms indicates a good capability to mediate visible photon–electron conversion processes. Porphyrins and related macrocycles such as phthalocyanines provide an extremely versatile synthetic base for a variety of materials for applications in many disciplines of chemistry and physics, such as opto-electronics, electrochemistry, catalysis, data storage, and solar cells [4,10,58–60]. Porphyrins and metalloporphyrins have also been examined for a variety of applications as sensors, which clearly represent an important class of chemo-responsive materials [10,22,61]. The stability of mono- and di-cation porphyrin π-radicals makes these systems especially interesting for photoionization processes, closely related to the so-called special pair reaction center of photosynthesis [4,9].

Fullerene–porphyrin mixed systems have recently become an active area of research for the generation of photocurrent [62–64]. To reveal the elemental processes, including electron transfer and electron-mediation process in addition to energy transfer (EN), there are several studies available in the literature [65–71]. Supramolecular systems composed of functionalized fullerenes that are coordinated to the central metal of the porphyrin have been studied to mimic the photosynthetic system [72–81]. The covalently connected fullerene–porphyrin dyads and triads were extensively investigated with the purpose of generating photocurrent, in addition to their unique photophysical and photochemical properties [48–52].

In the first part of the present review, we focus on the intermolecular ET between fullerenes (C_{60} and C_{70}) with porphyrins, chlorophylls, phthalocyanines and naphthalocyanines to reveal the fundamental photochemical features of these systems. In the second part, we summarize the photochemical behavior of supramolecular assemblies, in which functionalized fullerenes are noncovalently interacting with porphyrins and phthalocyanines.

2. Intermolecular electron transfer

The simplest way to prepare the intermolecular system is by mixing electron acceptors (fullerenes) with electron donors (porphyrins, chlorophylls, phthalocyanines, and naphthalocyanines) in a suitable solvent. The electron transfer events can be monitored by observing the radical ions by means of nanosecond transient absorption spectra in the visible and near-IR regions, with which the ET mechanism and ET kinetics can be characterized. We have organized this section into four parts: The first part deals with the ET processes of C_{60} and C_{70} with tetraphenylporphyrin (H_2TPP) bearing different substituents on the phenyl rings. The second part covers the ET processes of C_{60} and C_{70} with metal octaethylporphyrins (MOEP, where M = H_2, Pd, Ni, Co, V=O, Mg, Zn and Cu) to probe the effect of metal ions in the porphyrin cavity. The third part deals with the ET processes of C_{60} and C_{70} with chlorophylls (Chls) to reveal the role in natural systems. Finally, the fourth part deals with the ET processes of C_{60} and C_{70} with phthalocyanines (Pc) and naphthalocyanines (Nc) to probe structural effects of electron donors.

2.1. Fullerenes–tetraphenylporphyrins

Recently, we studied the electron transfer process of C_{60} with tetraphenylporphyrin (H_2TPP) bearing different substituents on the phenyl rings to probe the substituent effects on the rates of the electron transfer process. It was reported that the photophysical and photochemical properties of porphyrins are affected by the substituents [82–85].

We employed free-base tetraphenylporphyrin (H_2TPP), tetra(*p*-hydroxyphenyl)-porphyrin (H_2THPP) and tetra(*p*-aminophenyl)porphyrin (H_2TAPP) and tetra(*p*-methoxyphenyl) porphyrin (H_2TMPP) as electron donors (Fig. 2) with C_{60} as an electron acceptor. This study was carried out in benzonitrile (BN) via triplet states of porphyrins ($^3H_2$TPPs*) by observing the transient spectra in the wide spectral range from 400 to 1500 nm.

The absorption spectra of H_2TPP, H_2THPP and H_2TAPP are shown in Fig. 3. The absorption bands of the porphyrins with electron-donating substituents are shifted to longer wavelength compared with those of H_2TPP (Fig. 3). Such red shifts might originate from the narrowing of the band gap energy, which is caused by an increase in the HOMO energy level with electron-donating substituents, as can be interpreted according to Gouterman's four orbital model [86].

Absorption spectra of C_{60} and C_{70} are shown in Fig. 4; the absorbance in the visible region of C_{60} is weaker than those of H_2TPP derivatives. The absorption spectra of the mixture of either of H_2TPP, H_2THPP, or H_2TAPP with C_{60} are the same as the summation of the spectra of the corresponding components, suggesting that the interaction between C_{60} and the substituted porphyrins in the ground state is weak.

By photoexcitation of H_2TPP (0.1 mM) in deaerated BN using a 550 nm laser, the transient absorption spectrum obtained immediately after the laser pulse exhibited absorption bands at 450 and 780 nm, which are assigned to the triplet state of H_2TPP ($^3H_2$TPP*) [69–71]. In the presence of C_{60}, the generation of $C_{60}^{\bullet -}$ was observed by a build-up of the absorption at 1080 nm at 10 μs [32,33,45–47] that parallels a concomitant decay of $^3H_2$TPP* (Fig. 5a). It was difficult to observe clearly the $H_2TPP^{\bullet +}$ at 650 nm, because of the overlap with the depletion and emission of H_2TPP. In

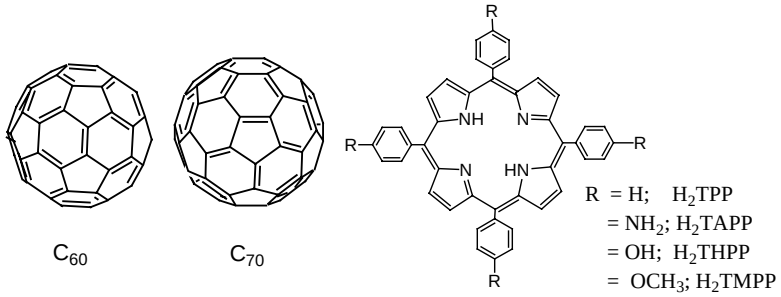

Fig. 2. Structures of C_{60}, C_{70} and *meso*-tetraphenylporphyrins.

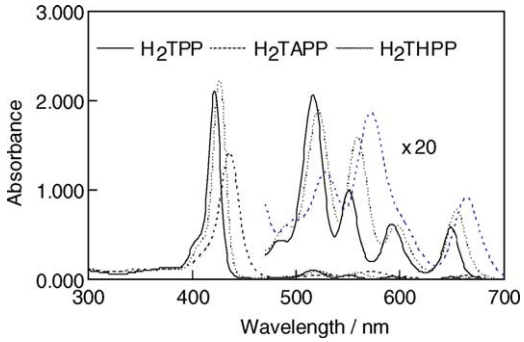

Fig. 3. Steady state absorption spectra of H_2TPP, H_2TAPP, and H_2THPP in BN; concentration = 0.007 mM.

the case of H_2TAPP as an electron donor to C_{60}, the transient spectrum (Fig. 5b) showed the bands at 460, 630, and 740 nm immediately after the laser exposure. These three bands are clearly assigned to $^3H_2$TAPP*. With the decay of $^3H_2$TAPP*, the rise of $C_{60}^{\bullet-}$ was observed at 1080 nm. Interestingly, the broad absorption bands in the 600–1400 nm region with maxima at 580, 780, and 1200 nm, which are attributed to $H_2TAPP^{\bullet+}$, were observed in the spectrum at 10 μs. Similarly, with the decays of $^3H_2$THPP* at 460, 620, and 680 nm, the rise of $H_2TPP^{\bullet+}$, showing absorptions at 630, 680 and 950 nm, was observed in addition to $C_{60}^{\bullet-}$ at 1080 nm (Fig. 5c).

Furthermore, the contribution of the triplet states of porphyrins to the ET process was confirmed by the O_2 effect.

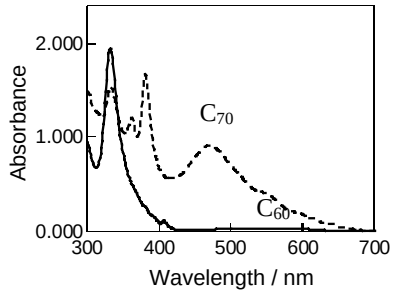

Fig. 4. Steady state absorption spectra of C_{60} and C_{70}; concentration = 0.1 mM.

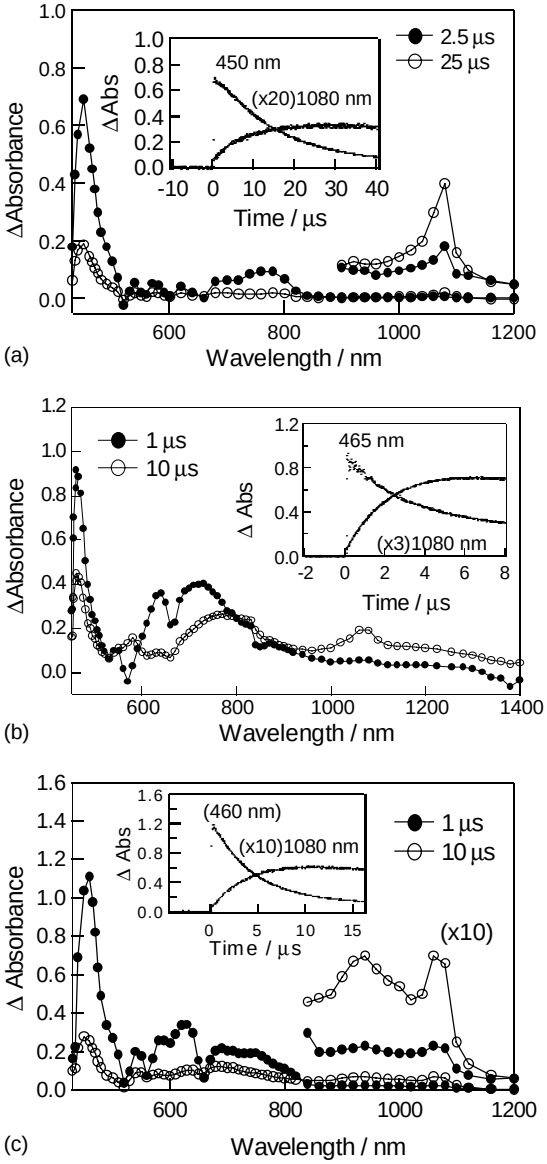

Fig. 5. Transient absorption spectra obtained by 550 nm laser photolysis of (a) H_2TPP (0.1 mM), (b) H_2TAPP (0.1 mM), and (c) H_2THPP in the presence of C_{60} (0.1 mM) in Ar-saturated BN.

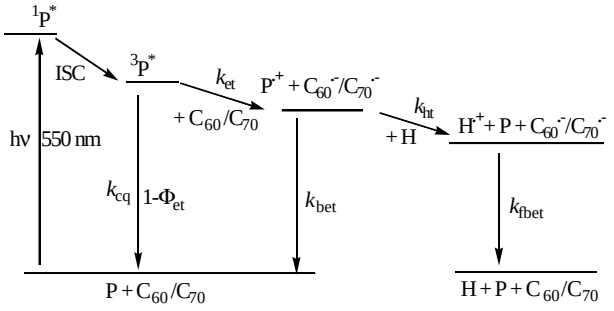

Fig. 6. Energy diagram for electron transfer by photoexcitation of P, which represents porphyrins, phthalocyanines, and chlorophylls, in the presence of C_{60}/C_{70} in polar solvents.

On addition of O_2, the decay of $^3H_2TPP^*$ was accelerated owing to energy transfer to O_2; consequently, the formation of $C_{60}^{\bullet-}$ and $H_2TPPs^{\bullet+}$ was suppressed. These observations suggest that the ET process takes place from $^3H_2TPP^*$ to C_{60} (Fig. 6).

A more detailed picture of the kinetic event was observed in the time profiles, from which the rate constants of the bimolecular quenching (k_q) of $^3H_2TPP^*$ were evaluated by monitoring the first-order decays of $^3H_2TPPs^*$ as a function of C_{60} concentrations under the condition of $[^3H_2TPPs^*] \ll [C_{60}]$. The first-order rate constant for the decays of $^3H_2TPPs^*$ in the presence of C_{60} is referred to as k_{1st} in Eq. (1).

$$k_{1st} = k_0 + k_q[C_{60}] \quad (1)$$

where k_0 is referred to as a rate constant for the decay of $^3H_2TPPs^*$ in the absence of C_{60}. The linear dependence of the observed k_{1st} values on $[C_{60}]$ gives the rate constant for bimolecular quenching (k_q), as summarized in Table 1. The k_q values of $^3H_2TPPs^*$–C_{60} are in the range of $(1.1–1.3) \times 10^9\ M^{-1}\ s^{-1}$, although larger k_q values were expected for substituted porphyrins, because of the lower oxidation potential (E_{ox}) values of substituted porphyrins, H_2TMPP (0.98 V), H_2THPP (0.75 V), and H_2TAPP (0.48 V) compared to H_2TPP (1.05 V) versus Fc/Fc^+ [87–89].

For $^3H_2TPP^*$, the absorption of $C_{60}^{\bullet-}$ was not overlapped with those of the radical cation of $H_2TPP^{\bullet+}$; therefore we can evaluate the maximal concentration of $C_{60}^{\bullet-}$ from the reported molar extinction coefficient ($14{,}000\ M^{-1}\ cm^{-1}$ at 1080 nm) [45–47,69–71]. In contrast, the initial concentration of $^3H_2TPP^*$ was also evaluated from the molar extinction coefficient ($20{,}000\ M^{-1}\ cm^{-1}$ at 450 nm) [90]. Thus, the efficiency of ET via $^3H_2TPP^*$ can be evaluated from the ratio of $[C_{60}^{\bullet-}]_{max}/[^3H_2TPP^*]_{initial}$, which usually saturates at appropriately high concentrations of $[C_{60}]$. The saturated ratio can be made equal to the quantum yield (Φ_{et}); for $^3H_2TPP^*$–C_{60}, the Φ_{et} value was evaluated to be 0.26 [71]. The rate constants for electron transfer (k_{et}) can be evaluated with Eq. (2) [91–93]:

$$k_{et} = \Phi_{et} k_q \quad (2)$$

Since the Φ_{et} values are less than unity, there may be bimolecular deactivation processes of $^3H_2TPP^*$ other than the ET process. As such a bimolecular deactivation process of $^3H_2TPP^*$, collisional quenching can be considered, as shown in Scheme 1, since energy transfer processes were not observed.

For $^3H_2TAPP^*$–C_{60}, $^3H_2THPP^*$–C_{60}, and $^3H_2TMPP^*$–C_{60}, the molar extinction coefficients were not exactly evaluated; thus, the values of Φ_{et} and k_q have not yet been obtained. Thus, the substituent effect on values of Φ_{et} and k_q is not clear at this moment.

In the long time scale measurements, it was clearly observed that $C_{60}^{\bullet-}$ begins to decay slowly after reaching the maximal absorbance. The decay time profile was fitted with second-order kinetics, suggesting that a bimolecular back ET process (k_{bet}) from $C_{60}^{\bullet-}$ to $TAPP^{\bullet+}$ takes place after these radical ions are solvated separately into free radical ions in a polar solvent such as BN.

$$\frac{1}{\Delta A_t} = \frac{1}{\Delta A_0} + \frac{k_{bet}}{\varepsilon} t \quad (3)$$

From the slopes of the line of the second-order plot of $1/\Delta A_t$ versus time (t), the ratio of the back ET rate constant (k_{bet}) to the molar extinction coefficient of the radical ions (ε) can be obtained. On employing the reported extinction coefficient (ε_A) of $C_{60}^{\bullet-}$, the k_{bet} values were evaluated, as listed in Table 1. The k_{bet} values of the substituted systems $C_{60}^{\bullet-}$–$H_2TAPP^{\bullet+}$, $C_{60}^{\bullet-}$–$H_2THPP^{\bullet+}$, and $C_{60}^{\bullet-}$–$H_2TMPP^{\bullet+}$ are much smaller than that of $C_{60}^{\bullet-}$–$H_2TPP^{\bullet+}$, suggesting the delocalization of the hole in the substituted porphyrins,

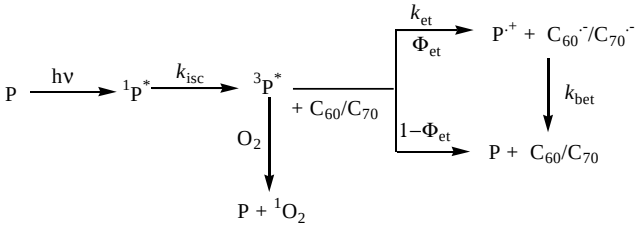

Scheme 1. Routes for ET process occurring by the photoexcitation of electron donors (P) in the presence of fullerenes (C_{60}/C_{70}) in BN; P is an abbreviation for porphyrins, chlorophylls, phthalocyanines, and naphthalocyanines.

Table 1
Quenching rate constants (k_q) of the excited triplet states of substituted tetraphenylporphyrins ($^3TPPs^*$) by fullerene (C_{60}) and back electron transfer rate constants (k_{bet}) between $C_{60}^{\bullet-}$ and $P^{\bullet+}$ in Ar-saturated benzonitrile (BN)

Systems	k_q ($M^{-1}s^{-1}$) ($\times 10^9$)	k_{bet} ($M^{-1}s^{-1}$) ($\times 10^9$)
$^3H_2TAPP^*$–C_{60}	1.1	2.4
$^3H_2THPP^*$–C_{60}	1.4	3.5
$^3H_2TMPP^*$–C_{60}	1.3	5.5
$^3H_2TPP^*$–C_{60}[a]	1.1	4.9

[a] $\Phi_{et} = 0.26$ and $k_{et} = 2.9 \times 10^8\ M^{-1}\ s^{-1}$ [69].

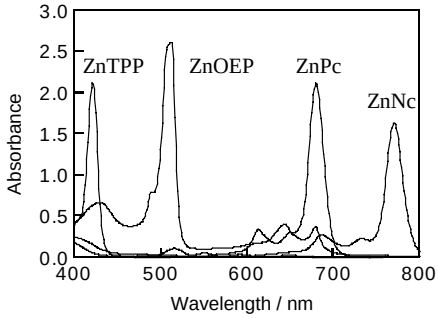

Fig. 7. Steady state absorption spectra of zinc tetraphenylporphyrin (ZnTPP), zinc octaethylporphyrin (ZnOEP), zinc phthalocyanine (ZnPc) and zinc naphthalocyanines (ZnNc) in BN: concentration = 0.007 mM.

which is supported by the appearance of the longer wavelength absorption band of $H_2TAPP^{\bullet+}$, $H_2THPP^{\bullet+}$, and $H_2TMPP^{\bullet+}$. In general, the k_{bet} values seem to be close to the diffusion-controlled limit (k_{diff}) in BN, which means that $C_{60}^{\bullet-}$ and $H_2TPP^{\bullet+}$ are long lived, although the lifetimes were dependent on their concentration [89]. Since the concentrations of $C_{60}^{\bullet-}$ and $H_2TPP^{\bullet+}$ are considerably lower than that of the reactant [C_{60}], the observed decay rates of the backward process are far smaller than that of the forward process, even though $k_{bet} \gg k_{et}$.

The PET process was investigated between MTPP (M = H_2, Zn, Cu) and fullerenes (C_{60}/C_{70}) in polar solvents by applying the 532 nm nanosecond laser photolysis method [69,70]. As shown in Fig. 7, the absorption peaks of ZnTPP are almost the same as those of H_2TPP. The ET process was followed via both ^{3}MTPP* and $^3C_{60}{}^*/^3C_{70}{}^*$ by controlling the excitation molecules by their absorbance at 532 nm.

By employing the laser light at 532 nm, selective excitation of C_{70} was possible, since the absorption intensity at 532 nm of C_{70} is much higher than those of MTPP. The transient absorption of $^3C_{70}{}^*$ appeared at 980 nm immediately after the laser light excitation of C_{70} in the presence of excess MTPP. With concomitant decay of $^3C_{70}{}^*$, the transient absorption band of $C_{70}^{\bullet-}$ appeared at 1380 nm in the near-IR region giving evidence of ET from ZnTPP to $^3C_{70}{}^*$ in BN. Similarly, ET from ZnTPP to $^3C_{60}{}^*$ was possibly investigated at high concentration of $^3C_{60}{}^*$ to permit the selective excitation of $^3C_{60}{}^*$. Fig. 8 shows the schematic energy diagram of the ET process from the ground state of ZnTPP to $^3C_{60}{}^*/^3C_{70}{}^*$.

Table 2
Quenching rate constants (k_q), electron transfer quantum yield (Φ_{et}) electron transfer rate constants (k_{et}) of fullerene–MTPP systems in BN

Systems	k_q ($M^{-1}\,s^{-1}$) ($\times10^9$)	Φ_{et}	k_{et} ($M^{-1}\,s^{-1}$) ($\times10^8$)
$^3C_{70}{}^*$–ZnTPP	2.2	0.35	7.7
$^3C_{60}{}^*Z$–ZnTPP	4.3	0.26	1.1
$^3C_{60}{}^*$–CuTPP	2.1	0.13	2.7
^{3}ZnTPP*–C_{70}	4.7	0.15	7.0
^{3}ZnTPP*–C_{60}	4.0	0.12	4.8

The quantum yields (Φ_{et}) via $^3C_{60}{}^*$ and $^3C_{70}{}^*$ can be evaluated from the ratio of $[C_{60}^{\bullet-}]_{max}/[^3C_{60}{}^*]_{initial}$ and $[C_{70}^{\bullet-}]_{max}/[^3C_{70}{}^*]_{initial}$ in the range of 0.2–0.4, which also suggests the presence of the collisional quenching of $^3C_{60}{}^*$ and $^3C_{70}{}^*$ without ET (Scheme 2). The k_{et} values for $^3C_{60}{}^*$ and $^3C_{70}{}^*$ from ZnTPP and CuTPP were evaluated from k_q Φ_{et}, as listed in Table 2.

In concentrated solutions of ZnTPP in which it was photoexcited selectively by 532 nm laser light, ET takes place from ^{3}ZnTPP* to the ground state of C_{60} and C_{70}, producing $C_{60}^{\bullet-}$ and $C_{70}^{\bullet-}$ (Scheme 1). The electron transfer rate constants and efficiencies were evaluated, listed in Table 2. Although there were slight differences in the k_q, Φ_{et}, and k_{et} values between C_{60} and C_{70} as well as between ZnTPP and H_2TPP, it can be considered that they are substantially similar values. This implies that the rigorous removal of C_{70} from mixtures of C_{60} and C_{70} is not necessary.

2.2. Fullerenes–octaethylporphyrins [70,93]

This section covers the ET process of metal octaethylporphyrins (MOEP, where M= H_2, Pd, Ni, Co, V=O, Mg, Zn and Cu) with fullerenes (C_{60}/C_{70}) to reveal the effect of the metal ions in the porphyrin cavity (Fig. 9). Steady-state absorption bands of ZnOEP appear at longer wavelengths than those of ZnTPP, as shown in Fig. 7. The insertion of metal atoms into OEP usually strongly changes the visible absorption spectra; i.e., the Q-bands of H_2OEP (498,

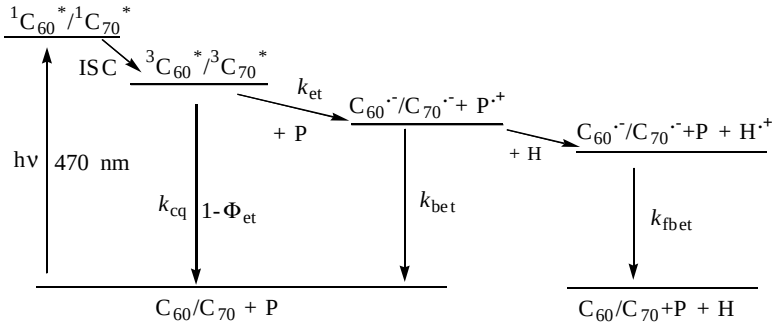

Fig. 8. Energy diagram for electron transfer by photoexcitation of fullerenes (C_{60}/C_{70}) in the presence of porphyrins (P) in polar solvents.

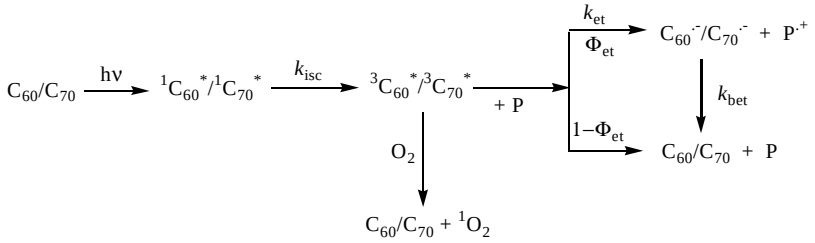

Scheme 2. Routes for the ET process occurring by the photoexcitation of fullerenes (C_{60}/C_{70}) in the presence of porphyrins (P) in BN.

532, 567, and 521 nm), PdOEP (512, 546 nm), NiOEP (517, 552 nm), CuOEP (526, 562 nm), (V=O)OEP (534, 572 nm) and MgOEP (544 and 579 nm).

Selective excitation of C_{70} is possible even in the presence of excess MOEP by 470 nm laser light irradiation. In the transient absorption spectra obtained immediately after the laser excitation, the absorption band of $^3C_{70}$* at 980 nm was solely observed; with concomitant decay of $^3C_{70}$*, the absorption of $C_{70}^{\bullet-}$ appeared at 1380 nm with the absorption of $MOEP^{\bullet+}$ at 650 nm, indicating that the ET process takes place in the same manner, as shown in Fig. 8.

The ET quantum yields (Φ_{et}) of $C_{70}^{\bullet-}$ formation via $^3C_{70}$* were evaluated from $[C_{70}^{\bullet-}]_{max}/[^3C_{70}^*]_{initial}$ at appropriately high concentrations of [MOEP]. The Φ_{et} values via $^3C_{70}$* varied with the central metal according to the following order; PdOEP > MgOEP > ZnOEP > (V=O)OEP > CoOEP > NiOEP > CuOEP. The change in the donor abilities of the MOEPs may be explained mainly by their E_{ox} values. The observed Φ_{et} values are less than unity, suggesting that there are some deactivation routes (e.g., collisional quenching and/or an encounter complex). The possibility of EN from $^3C_{70}$* to MOEP in BN solution is quite low, because the rise of ^{3}MOEP* was not observed. Thus, the deactivation process may be attributed to collisional quenching.

In Table 3, it is shown that the Φ_{et} values gradually increase with decreasing $E_{ox}(D/D^+)$, except for (V=O)OEP. The free energy changes (ΔG^0_{et}) for ET from ^{3}P to C_{60} were calculated from the Rehm–Weller relation [16,17].

$$\Delta G^0_{et} = E_{ox}(D/D^{\bullet+}) - E_{red}(A^{\bullet-}/A') - E_T - E_c \quad (4)$$

where $E_{ox}(D/D^{\bullet+})$, $E_{red}(A^{\bullet-}/A)$, E_c and E_T refer to the oxidation potential of the donor, the reduction potential of the acceptor (C_{60}/C_{70}), the Coulomb term, and the triplet energy of the excited species, respectively. It was also observed that the k_{et} values increase with decreasing ΔG^0_{et} values along the curve calculated by the semiempirical Rehm–Weller plot [16,17]. For systems with very negative ΔG^0_{et} values, the k_{et} values are close to k_{diff} in BN [89]. The k_{bet} values in BN listed in Table 3 are also close to k_{diff}, because the free energy change (ΔG^0_{bet}) for back ET from $C_{70}^{\bullet-}$ to $MOEP^{\bullet+}$, which can be calculated from Eq. (5), are all very negative.

$$\Delta G^0_{bet} = E_{ox}(D/D^{\bullet+}) - E_{red}(A^{\bullet-}/A) - E_c \quad (5)$$

By laser excitation of C_{70} in the presence of MOEP in toluene, no ET process was observed. The EN process from $^3C_{70}$* to MOEP in toluene was also not observed; this observation is reasonable, because E_T ($^3C_{70}^* = 1.54$ eV) is slightly lower than E_T (^{3}MOEP* = 1.60–1.90 eV). Thus, the formation of the triplet exciplex $^3[C_{70}^{(\delta-)} \cdots MOEP^{(\delta+)}]^*$ would be expected to be dominant in nonpolar solvents. The formation of such triplet exciplexes in nonpolar solvents has been reported during the quenching of ^{3}MTPP by various quinones in toluene [94]. Thus, the formation of $^3[C_{70}^{(\delta-)} \cdots MOEP^{(\delta+)}]^*$ could provide a possible explanation for the near diffusion-controlled triplet quenching rate constant of $^3C_{70}$* in the presence of MOEP in toluene.

Kinetic analysis of the $^3C_{70}$*–MgOEP system in toluene–BN mixtures afforded valuable information about the dissociation of $^3[C_{70}^{(\delta-)} \cdots MOEP^{(\delta+)}]^*$ into the

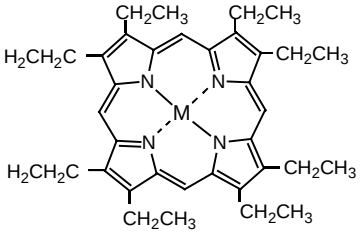

Metal octaethylporphyrins (MOEP)
(M = Pd, Mg, Zn, Co, Ni, Cu and (V=O)

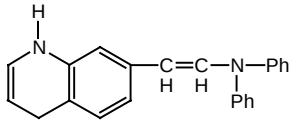

N,N-diphenyl-N-(1,2,3,4-tetrahydro-quinoline-6-yl-methylene)hydrazine (DTQH)

Fig. 9. Structure of metal octaethylporphyrins (MOEP) and a hole-transfer reagent (DTQH).

Table 3
Oxidation potentials (E_{ox}), and free energy changes (ΔG^0_{et}), and kinetic parameters (k_q, Φ_{et} and k_{et}) for the ET process from MOEP via $^3C_{70}$* in BN; k_{bet} between $C_{70}^{\bullet-}$ and $MOEP^{\bullet+}$

System	E_{ox} (V)	ΔG^0_{et} (kJ mol^{-1})	k_q (M^{-1} s^{-1})	Φ_{et}	k_{et} (M^{-1} s^{-1})	k_{bet} (M^{-1} s^{-1})
$^3C_{70}$*–PdOEP	0.44	−66.5	2.2×10^9	0.74	1.6×10^9	3.2×10^9
$^3C_{70}$*–MgOEP	0.53	−57.7	2.4×10^9	0.52	1.2×10^9	4.7×10^9
$^3C_{70}$*–ZnOEP	0.63	−48.1	2.9×10^9	0.40	1.1×10^9	9.0×10^9
$^3C_{70}$*–NiOEP	0.64	−47.3	2.7×10^9	0.32	8.7×10^8	6.5×10^9
$^3C_{70}$*–CoOEP	0.68	−43.5	2.2×10^9	0.39	8.5×10^8	4.0×10^9
$^3C_{70}$*–CuOEP	0.85	−27.2	2.0×10^9	0.21	4.3×10^8	8.0×10^9
$^3C_{70}$*–(V=O)OEP	0.96	−17.2	1.8×10^9	0.40	7.2×10^8	4.6×10^9
$^3C_{60}$*Z–NiOEP	0.64	−43.5	3.5×10^9	0.11	3.9×10^8	1.2×10^9
$^3C_{60}$*Z–CoOEP	0.68	−27.2	3.3×10^9	0.11	3.6×10^8	7.8×10^9
$^3C_{60}$*Z–CuOEP	0.85	−18.8	2.6×10^9	0.06	1.6×10^8	9.7×10^9

Table 4
Kinetic parameters (k_q, Φ_{et}, and k_{et}) for the ET process via $^3C_{70}$* in the presence of (V=O)OEP and k_{bet} between $C_{70}^{\bullet-}$ and $(V=O)OEP^{\bullet+}$ in Ar-saturated BN:toluene (Tol) mixtures

Solvents (BN:Tol)	k_q (M^{-1} s^{-1})	Φ_{et}	k_{et} (M^{-1} s^{-1})	k_{bet} (M^{-1} s^{-1})
25:75	3.3×10^9	–	–	–
50:50	3.3×10^9	0.25	8.3×10^8	9.7×10^9
60:40	3.3×10^9	0.30	9.8×10^8	7.4×10^9
75:25	3.0×10^9	0.35	1.1×10^9	5.6×10^9
87:13	2.8×10^9	0.39	1.1×10^9	5.3×10^9
100:0	2.6×10^9	0.40	1.1×10^9	4.5×10^9

solvent-separated ion-pair (SSIP) or into free radical ions in solution. In the region of toluene-rich content (toluene > 75%), the rapid decay of the transient absorption band of $^3C_{70}$* was observed with formation of $C_{70}^{\bullet-}$, similar to that of 100% toluene solution. Thus, it is assumed that less polar solvents retard the dissociation of the triplet exciplex into SSIPs or into free radical ions in solution. In the region BN > 25%, the dissociation of the triplet exciplex was confirmed by observing the absorption bands of $C_{60}^{\bullet-}/C_{70}^{\bullet-}$ and $MOEP^{\bullet+}$. This is reasonably interpreted by the stabilization of the SSIP and free radical ions in a polar medium. In polar solvents, on assuming that lifetimes of $^3[C_{70}^{(\delta-)} \cdots MOEP^{(\delta+)}]$* are very short, the Φ_{et} and k_{et} values can be evaluated in a similar manner to those of BN, as listed in Table 4. In both BN and toluene–BN, the decay of $C_{60}^{\bullet-}/C_{70}^{\bullet-}$ and $MOEP^{\bullet+}$ was fitted with second-order kinetics, suggesting that the radical ions are present as free ion radicals or SSIP. The evaluated k_{bet} values (Table 4) seem to increase slightly with increasing toluene fraction. This finding suggests that the fraction of SSIP increases with toluene fraction, resulting in the increase of k_{bet} values.

By employing laser light at 560 nm, selective excitation of MOEP was possible even in the presence of C_{60} and C_{70}; thus, the ET process via ^{3}MgOEP* was confirmed by observing the decay of the absorption bands of ^{3}MOEP* at 440 nm and the concomitant rise of $C_{60}^{\bullet-}$ at 1080 nm and $C_{70}^{\bullet-}$ at 1380 nm. A possibility of the ET process via ^{1}MOEP* is excluded due to the slow rise of $C_{60}^{\bullet-}$ and $C_{70}^{\bullet-}$. The kinetic parameters for the ^{3}MOEP*–C_{60} systems in BN are listed in Table 5. The k_q values via ^{3}MOEP* are almost the same as those via $^3C_{70}$*/$^3C_{60}$*, which is reasonable on the basis of their similar ΔG^0_{et} values. It is remarkable that the Φ_{et} values via ^{3}MOEP*–C_{70} systems seem to be higher than those of the ^{3}MOEP*–C_{60} systems; the difference can be explained by the difference in the E_{red} values between C_{60} (−0.51 V versus SCE in BN) and C_{70} (−0.43 V versus SCE in BN).

The transient absorption spectrum observed after laser excitation of MgOEP in the presence of C_{70} and DTQH, which is well known as a hole shifter, confirmed the hole shift process from $MgOEP^{\bullet+}$ to DTQH, generating $DTQH^{\bullet+}$. Fig. 10 shows the transient absorption spectra observed by the selective excitation of MgOEP in the presence of C_{70} and DTQH in BN. At 0.5 μs, the sharp band at 440 nm of ^{3}MOEP* was observed, showing rapid decay

Table 5
Kinetic parameters (k_q, Φ_{et}, and k_{et}) for ET from ^{3}MOEP* to C_{60}/C_{70} in Ar-saturated BN; k_{bet} between $C_{60}^{\bullet-}/C_{70}^{\bullet-}$ and $MOEP^{\bullet+}$

System	k_q (M^{-1} s^{-1})	Φ_{et}	k_{et} (M^{-1} s^{-1})	k_{bet} (M^{-1} s^{-1})
^{3}PdOEP*–C_{60}	3.2×10^9	0.47	1.5×10^9	7.3×10^9
^{3}ZnOEP*–C_{60}	3.7×10^9	0.28	1.0×10^9	8.4×10^9
^{3}MgOEP*–C_{60}	3.1×10^9	0.21	6.5×10^8	9.9×10^9
^{3}(V=O)OEP*–C_{60}	3.2×10^9	0.19	6.0×10^8	4.5×10^9
^{3}PdOEP*–C_{70}	3.3×10^9	0.60	2.0×10^9	3.3×10^9
^{3}ZnOEP*–C_{70}	3.0×10^9	0.49	1.5×10^9	8.9×10^9
^{3}MgOEP*–C_{70}	2.0×10^9	0.40	8.0×10^8	4.8×10^9
^{3}(V=O)OEP*–C_{70}	2.0×10^9	0.25	5.0×10^8	4.5×10^9

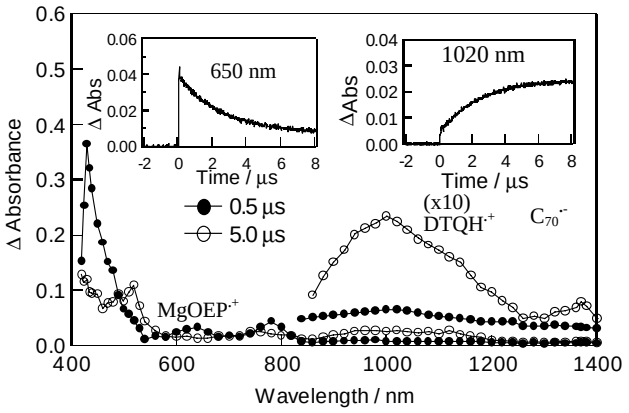

Fig. 10. Transient absorption spectra observed by 550 nm laser excitation of MgOEP (0.1 mM) in the presence of C_{70} (0.1 mM) and DTQH (5 mM) in Ar-saturated BN. Inset: time profiles at 650 and 1020 nm [93].

by ET to C_{70}, producing $C_{70}^{\bullet-}$ at 1380 nm. Although, the absorption of $MgOEP^{\bullet+}$ appeared at 640 nm in the absence of DTQH, in its presence, the rapid decay of $MgOEP^{\bullet+}$ was observed, with concomitant rise of $DTQH^{\bullet+}$ in the 800–1300 nm region. Thus, photosensitized ET occurs at first from $^3MgOEP^*$ to C_{70}, yielding $C_{70}^{\bullet-}$ and $MgOEP^{\bullet+}$, followed by the hole shift from $MgOEP^{\bullet+}$ to DTQH, yielding $DTQH^{\bullet+}$, as summarized in Scheme 3. Such a hole shift is possible when the E_{ox} value of the hole shift reagent DTQH ($E_{ox} = 0.32$ V versus SCE) is lower than that of MgOEP ($E_{ox} = 0.53$ V versus SCE). The final back ET rate constant (k_{fbet}) was evaluated as $6.1 \times 10^8\ M^{-1}\ s^{-1}$ by following the long time decay profiles of $DTQH^{\bullet+}$ and $C_{70}^{\bullet-}$, which obey second-order kinetics. The decay of $C_{70}^{\bullet-}$ in the presence of $DTQH^{\bullet+}$ ($k_{fbet} = 6.1 \times 10^8\ M^{-1}\ s^{-1}$) is slowed down compared with that in the presence of $MgOEP^{\bullet+}$ ($k_{bet} = 4.7 \times 10^9\ M^{-1}\ s^{-1}$).

2.3. Fullerene–chlorophylls [95]

In photosynthesis, the chlorophylls, Chls (close cousins of metalloporphyrins) play key roles in absorbing light energy over a wide spectral range and converting the light energy into the highly directional transfer of electrons. Green plants employ chlorophylls and magnesium–chlorins as the chromophores to harvest light. The investigations of oxidation–reduction reactions photosensitized by Chls in vitro are of great importance to elucidate the mechanism of the primary photoreactions in photosynthesis [96,97].

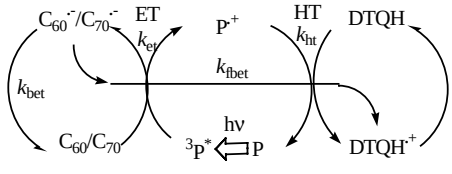

Scheme 3. Routes for the electron-transfer/hole shift cycle start with photoexcitation of P in the presence of C_{60}/C_{70} and DTQH in Ar-saturated BN.

One of the specific features of Chls is related to the quenching of their photoexcited states by compounds with high electron affinity via an ET process [99,100]. The quenching of excited states of Chls by quinones has been widely studied as a simple model system for the primary photoinduced CS in the chloroplast. It has been demonstrated by the flash photolysis and ESR techniques that various quinones quench $^3Chls^*$. By ESR measurements, the signal of the semiquinone ($Q^{\bullet-}$) was observed [98,99]. Also, by applying laser flash photolysis measurements, the intermediates $Q^{\bullet-}$ and $Chls^{\bullet+}$ were observed by the light excitation of Chls. The main problem frequently faced in the flash photolysis measurements is the overlap of the absorptions of the intermediates, which leads to difficulties in the interpretation of the mechanisms and quantitative analysis of the rates and yields of the ET processes. The absorption region of the Chls strongly overlaps with the absorption band of $Q^{\bullet-}$ at 435 nm. In addition, the absorption of $^3Chls^*$ masks most of the absorption band of the $Chls^{\bullet+}$ in the visible region. In contrast with quinones, the transient absorptions of $C_{60}^{\bullet-}$ and $C_{70}^{\bullet-}$ in the near-IR region make it easy to study quantitatively the elemental steps in the PET processes [95].

A considerable insight into the details of the ET process in the systems of Chl-a/Chl-b and C_{60}/C_{70} via $^3Chls^*$ can be obtained by applying 640 nm laser light, which selectively excites Chl-a/Chl-b. The transient absorption bands appeared at 480–500 nm, which are assigned unambiguously to $^3Chls^*$ [96–100].

In the presence of C_{60}/C_{70}, the ET processes from $^3Chl\text{-}a^*/^3Chl\text{-}b^*$ to C_{60}/C_{70} were observed by recording the diagnostic peaks of $C_{60}^{\bullet-}/C_{70}^{\bullet-}$ in the near-IR region by the excitation of Chl-a/Chl-b. The second-order quenching rate constant (k_q), ET quantum-yield (Φ_{et}), and ET rate constant (k_{et}) were evaluated, as in Table 6, in which the k_{et} values from $^3Chl\text{-}a^*$ to C_{60}/C_{70} are slightly larger than the corresponding values from $^3Chl\text{-}b^*$ to C_{60}/C_{70}. The difference in the E_{ox} and E_T values between Chl-a and Chl-b may be responsible for the difference in the k_{et} values. Moreover, the presence of the electron-withdrawing group (–CHO) decreases the electron-donor ability of Chl-b compared to Chl-a, with its electron-donating methyl group.

In benzene as a nonpolar medium, although rapid quenching of $^3Chl\text{-}a^*/^3Chl\text{-}b^*$ by C_{60}/C_{70} was observed, both ET and EN processes from $^3Chl\text{-}a^*/^3Chl\text{-}b^*$ to C_{60}/C_{70} are ruled out. This may be quite reasonable, because the E_T values of Chl-a/Chl-b are lower than those of C_{60} (1.5 eV). As a reason for the observed rapid quenching of $^3Chl\text{-}a^*/^3Chl\text{-}b^*$ by C_{60} in BZ, exciplex formation or collision deactivation may be considered.

By employing the excitation wavelength of the laser light at 532 nm, which selectively excites C_{70}, the ET process from Chl-a/Chl-b to $^3C_{70}^*$ was also confirmed in polar solvents. The transient spectra exhibited the absorption band

Table 6
Free energy changes (ΔG^0_{et}) and kinetic parameters (k_q, Φ_{et}, and k_{et}) for the ET process between Chl-a/Chl-b and (C_{60}/C_{70}) in BN and BZ

Systems	ΔG^0_{et} (kJ mol^{-1})	k_q (M^{-1} s^{-1})	Φ_{et}	k_{et} (M^{-1} s^{-1})	k_{bet} (M^{-1} s^{-1})
^{3}Chl-a*–C_{60}–BN	−31.4	1.9×10^9	0.44	8.4×10^8	1.0×10^{10}
^{3}Chl-a*–C_{70}–BN	−39.6	2.2×10^9	0.43	9.4×10^8	7.2×10^9
^{3}Chl-b*–C_{60}–BN	−27.5	1.9×10^9	0.20	3.8×10^8	4.5×10^9
^{3}Chl-b*–C_{70}–BN	−34.9	2.4×10^9	0.26	6.1×10^8	4.8×10^9
^{3}Chl-a*–C_{60}–BZ	–	2.2×10^9	–	–	–
^{3}Chl-a*–C_{70}–BZ	–	2.5×10^9	–	–	–
$^3C_{70}$*–Chl-a–BN	−55.7	2.2×10^9	0.37	8.1×10^8	8.8×10^9
$^3C_{70}$*–Chl-b–BN	−45.3	2.5×10^9	0.39	9.7×10^8	4.8×10^9
$^3C_{70}$*–Chl-a–BZ	–	3.4×10^9	–	–	–

of $^3C_{70}$* at 980 nm, which decayed with the concomitant formations of $C_{70}^{\bullet-}$ and Chl-b$^{\bullet+}$ at 1380 and 780 nm, respectively.

The high electron-donor abilities of Chl-a/Chl-b to $^3C_{70}$* and ^{3}Chl-a*/^{3}Chl-b* to C_{60}/C_{70} are in good agreement with the similarly high donor abilities of MgOEP and ZnOEP, as shown in Tables 3 and 5. We have come to conclude that Chls have similar electron-donor ability, in spite of their long chain, electron-withdrawing substituents and Mg(II) central atom.

2.4. Fullerenes–phthalocyanine/naphthalocyanine [70,101]

Phthalocyanines (Pc) are a class of organic compounds that have attracted great attention because of their unique properties, such as semiconductivity, photoconductivity, photochemical reactivity, chemical stability, electrochromism, bio-organic and catalytic activity and their various applications in technology [102–109].

Several studies have been performed to examine the photophysical properties as well as the potential for ET from metal phthalocyanines (MPc; M = H_2 and Zn in Fig. 11) to electron acceptor molecules. It has been reported that the photosensitivity of ZnPc in a polymeric binder is increased by the addition of C_{60} [110,111]. From photoemission experiments, C_{60} and C_{70} are expected to be appropriate electron-accepting materials when they are brought into contact with Pc in solids [63,64].

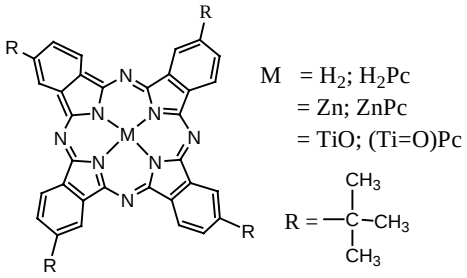

Fig. 11. Tetra-*t*-butylphthalocyanines.

In 1997, we reported a detailed study on the intermolecular ET between C_{60}/C_{70} and MPc via $^3C_{60}$*/$^3C_{70}$* by applying 532 nm nanosecond laser light in a polar solvent [70]. The selective excitation of C_{60}/C_{70} was possible in the presence of MPc, because MPc does not show any absorption at 532 nm at all. For example, the E_{ox} value of ZnPc generating ZnPc$^{\bullet+}$ is +0.8 V versus SCE in BN; thus, the ET process is possible from ZnPc to $^3C_{60}$*/$^3C_{70}$*. Indeed, excitation of C_{60}/C_{70} in BN gives rise to the rapid formation of $C_{60}^{\bullet-}/C_{70}^{\bullet-}$ at 1080 nm/1380 nm, and the rise of ZnPc$^{\bullet+}$ at 840 nm, with concomitant decay of $^3C_{60}$*/$^3C_{70}$* at 740 nm/980 nm. In contrast, in nonpolar solvents, although rapid quenching of $^3C_{60}$*/$^3C_{70}$* was observed in the presence of MPc, no evidence of formation of the radical ions was obtained by the nanosecond transient spectra, indicating absence of ET in the nonpolar solvent, because the energy levels for the radical ions are significantly raised. In the case of MPc, the evidence for EN was obtained by the rise of ^{3}MPc* at 490 nm, which is reasonable because of the lower E_T of MPc compared to that of $^3C_{60}$*/$^3C_{70}$*. These rate parameters are summarized in Table 7. It is noteworthy to mention that the ET quantum yield (Φ_{et}) via $^3C_{70}$* (0.75) was found to be higher than that via $^3C_{60}$* (0.50). Also, we proved that ZnPc acts as a stronger electron donor than H_2Pc [70]. In BZ, the energy transfer occurs predominantly even for ZnPc.

Further continuation of this study [101] was performed for the ET process via ^{3}MPc* to C_{60}/C_{70} by applying a 670 nm laser, which selectively excites MPc in the presence of excess C_{60}/C_{70}. In contrast to the porphyrins, we observed photoionization character of ZnPc in polar media. That is, the transient absorption spectrum with 670 nm laser light of ZnPc (0.1 mM) in BN exhibited absorption bands at 490 and 840 nm, corresponding to ^{3}ZnPc* and ZnPc$^{\bullet+}$, respectively. This indicated the occurrence of photoionization via ^{3}ZnPc* with a quantum yield (Φ_{ion}) less than 0.1 in BN. In the case of $^3H_2$Pc*, such photoionization did not occur even in polar solvents such as BN.

In the presence of C_{60}/C_{70}, the transient absorption spectra observed by excitation of ZnPc exhibited growth of the absorption bands of ZnPc$^{\bullet+}$ at 840 nm and $C_{60}^{\bullet-}/C_{70}^{\bullet-}$ at 1080 nm/1380 nm, accompanied by a concurrent decay of

Table 7
Kinetic parameters (k_q, Φ_{et}, and k_{et}) for electron transfer (ET) and energy transfer (EN) between $^3C_{60}^*/^3C_{70}^*$ and MPc in Ar-saturated BN and BZ

System	k_q ($M^{-1}\,s^{-1}$)	Φ_{et}	k_{et} ($M^{-1}\,s^{-1}$)	Φ_{en}	k_{en} ($M^{-1}\,s^{-1}$)
$^3C_{60}$*–ZnPc–BN	1.6×10^9	0.50	8.0×10^8	0.50	8.0×10^8
$^3C_{60}$*–ZnPc–BZ	2.1×10^9	0.00	–[a]	1.00	2.1×10^9
$^3C_{60}$*–H_2Pc–BN	3.0×10^9	0.18	5.4×10^8	0.82	2.5×10^8
$^3C_{60}$*–H_2Pc–BZ	2.8×10^9	0.00	–[a]	0.00	2.8×10^9
$^3C_{70}$*–ZnPc–BN	1.7×10^9	0.75	1.3×10^9	0.25	4.0×10^8
$^3C_{70}$*–ZnPc–BZ	1.8×10^9	0.00	–[a]	1.00	1.8×10^9
$^3C_{70}$*–H_2Pc–BN	3.5×10^9	0.20	7.0×10^8	0.80	2.8×10^8
$^3C_{70}$*–H_2Pc–BZ	1.8×10^9	0.00	–[a]	1.00	1.8×10^8

[a] No PET was observed.

^{3}ZnPc*. Furthermore, the rise rate of $ZnPc^{\bullet+}$ was quite similar to that of $C_{60}^{\bullet-}/C_{70}^{\bullet-}$. These findings indicate that ET takes place from ^{3}ZnPc* to C_{60}, with Φ_{et} = ca. 0.8, accompanied by only a small contribution from photoionization. The rate parameters are summarized in Table 8.

It was found that the k_q value of the ^{3}ZnPc*–C_{60} system ($8.7 \times 10^8\,M^{-1}\,s^{-1}$) is 300 times higher than that for the $^3H_2$Pc*–C_{60} system ($2.9 \times 10^6\,M^{-1}\,s^{-1}$). Moreover, we observed that the electron donor ability of ^{3}ZnPc* to C_{60} ($\Phi_{et} = 0.77$) is 10 times higher compared to $^3H_2$Pc* ($\Phi_{et} = 0.07$). In order to confirm whether such a large difference in electron donor ability between ^{3}ZnPc* and $^3H_2$Pc* was specific to the spherical fullerene molecule, we examined ET from ^{3}ZnPc* or $^3H_2$Pc* to benzoquinone (BQ) as a representative of flat small molecules. The results revealed that the higher electron donor ability is a general characteristic of ^{3}ZnPc* and $^3H_2$Pc*, but not a specific characteristic of the fullerene acceptors.

The ΔG_{et}^0 values evaluated for ET occurring from ^{3}ZnPc* and $^3H_2$Pc* to C_{60} were found to be −19.7 and −29.7 kJ mol^{-1}, respectively. Similarly for BQ, ΔG_{et}^0 values were calculated for ^{3}ZnPc* (−13.4 kJ mol^{-1}) and $^3H_2$Pc* (−17.2 kJ mol^{-1}). These negative ΔG_{et}^0 values imply that the k_{et} values via ^{3}ZnPc* and $^3H_2$Pc* to C_{60} (or C_{70} and BQ) are all close to the k_{diff} value ($5.6 \times 10^9\,M^{-1}\,s^{-1}$ in BN). However, the Φ_{et} values indicated that the electron acceptor ability of C_{70} is slightly lower than that of C_{60}, although the calculated ΔG_{et}^0 values did not predict such a tendency. The lower electron acceptor ability of C_{70} compared to C_{60} is also shown for $^3H_2$Pc* (Table 8). In nonpolar solvents, although quenching of ^{3}MPc* was observed, there was no evidence for ET and/or EN in the transient absorption spectra. The decay time profile of $C_{60}^{\bullet-}$ observed in the longer time scale obeyed second-order kinetics in BN, indicating that $ZnPc^{\bullet+}$ and $C_{60}^{\bullet-}$ recombine after being solvated as free radical ions. The k_{bet} values from $C_{60}^{\bullet-}$ and $C_{70}^{\bullet-}$ to $ZnPc^{\bullet+}$ in polar solvents were evaluated as being close to k_{diff}.

Recently, we reported the ET process in the systems composed of oxotitanium(IV) tetra-*t*-butyl-phthalocyanine ((Ti=O)Pc in Fig. 11) with C_{60} and C_{70} to examine the effect of the metal ion on the electron transfer process [112]. (Ti=O)Pc has been widely applied to the photoelectric conversion system, although it has low solubility in organic solvents. The absorption peaks, Soret and Q-bands, of (Ti=O)Pc were observed at 350 and 620–705 nm, respectively. The fluorescence time profile shows a single exponential decay, giving a lifetime of 5.1 ns. No dynamic quenching of ^{1}(Ti=O)P* was observed on addition of C_{60} or C_{70}, even in polar solvents.

The transient absorption spectra observed by the selective excitation of (Ti=O)Pc with laser light at 355 nm in Ar-saturated toluene exhibited the rapid decay of an absorption band at 1400 nm, with a rate of ca. $1 \times 10^8\,s^{-1}$, which may be assigned to the S_1–S_n transition of (Ti=O)Pc. With the decay band at 1400 nm, the growth of a band at 1300 nm

Table 8
Kinetic parameters (k_q, Φ_{et}, and k_{et}) for ET between ZnPc–BQ and C_{60}/C_{70} in Ar-saturated BN and BZ; k_{bet} between $C_{60}^{\bullet-}/C_{70}^{\bullet-}$ and $ZnPc^{\bullet+}/BQ^{\bullet+}$, k_q

System	k_q ($M^{-1}\,s^{-1}$)	Φ_{et}	k_{et} ($M^{-1}\,s^{-1}$)	k_{bet} ($M^{-1}\,s^{-1}$)
^{3}ZnPc*–C_{60}–BN	8.7×10^8	0.77	6.7×10^8	3.4×10^9
^{3}ZnPc* –C_{60}–BZ	6.3×10^8	0.00	–[a]	–[a]
^{3}ZnPc* –C_{70}–BN	1.6×10^9	0.48	7.7×10^8	3.3×10^9
^{3}ZnPc* –C_{70}–BZ	1.0×10^9	0.00	–[a]	–[a]
^{3}ZnPc* –BQ–BN	3.3×10^8	0.83	2.7×10^8	3.5×10^9
$^3H_2$TBPc*–C_{60}–BN	2.7×10^6	0.07	1.9×10^5	5.0×10^9
$^3H_2$Pc* –C_{60}–BZ	4.9×10^6	0.00	–[a]	–[a]
$^3H_2$Pc* –C_{70}–BN	$<10^5$	–[b]	–[b]	–[b]
$^3H_2$Pc* –BQ–BN	$<10^5$	–[b]	–[b]	–[b]

[a] No PET was observed.
[b] Too weak to observe or too slow to observe.

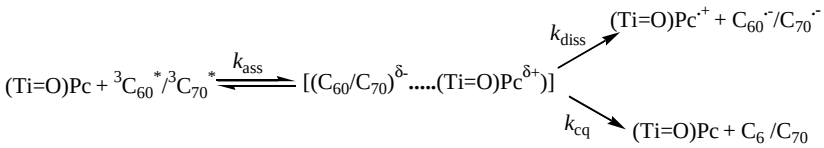

Scheme 4. Routes for the electron-transfer process occurring by the photoexcitation of C_{60}/C_{70} in the presence of (Ti=O)Pc in BN.

was observed. Since the species with absorption at 1300 nm has a long lifetime ($\tau = 67\,\mu s$), this species was attributed to ^{3}(Ti=O)Pc*. By the selective excitation of C_{70} and C_{60} in a nonpolar solvent, the EN process from $^3C_{70}$* and $^3C_{60}$* to (Ti=O)Pc was confirmed with rate constants of 3.3×10^9 and $2.0 \times 10^9\ M^{-1}\ s^{-1}$, respectively. This is the same tendency observed for MPc such as ZnPc and H_2Pc in Table 6 [70].

In polar BN solvent, the ET process from (Ti=O)Pc to $^3C_{60}$* was confirmed by observing the decay of $^3C_{60}$* at 750 with a concomitant rise of (Ti=O)Pc$^{\bullet+}$ at 880 nm and $C_{60}^{\bullet-}$ at 1080 nm. Similarly, the ET process was confirmed from (Ti=O)Pc to $^3C_{70}$*. The k_{1st} value of the rise of $C_{60}^{\bullet-}$ was found to be smaller than the k_{1st} value for the decay of $^3C_{60}$*, which might suggest some process intermediate between the decay and rise, such as triplet exciplex formation (Scheme 4).

The ΔG^0_{et} for ET from (Ti=O)Pc to $^3C_{60}$* was evaluated to be 0.64 eV by the Rehm–Weller equation. The Φ_{et} value via $^3C_{60}$* was evaluated as 0.2. Such a low Φ_{et} value for (Ti=O)Pc–$^3C_{60}$* system compared to ZnPc–$^3C_{60}$* system suggests the presence of a deactivation process of $^3C_{60}$* without ET; i.e., collisional quenching.

We have also investigated the ET process of the zinc tetra-*t*-butyl-naphthalocyanine (ZnNc in Fig. 12) and C_{60}/C_{70} systems via ^{3}ZnNc* to probe the structural effect on the ET process [113]. The steady-state absorption spectra of ZnNc appear at 780 nm (Fig. 7), which is at a longer wavelength compared to ZnTPP and ZnPc. Since C_{60} and C_{70} have no appreciable absorption intensity at 650 nm, ZnNc can be selectively excited by the 670 nm laser light. The transient absorption spectra of ZnNc in BN (Fig. 13a) exhibited the intense absorption bands of ^{3}ZnNc* at 600 and 770 nm accompanied by the weak growth of ZnNc$^{\bullet+}$ at 970 nm. As shown in the inset of Fig. 13a, the slow rise of ZnNc$^{\bullet+}$ at 970 nm seems to be a mirror image of the slow decay of ^{3}ZnNc* at 600 nm, suggesting that the photoionization takes place via ^{3}ZnNc*. In the presence of C_{60}, the ET process from ^{3}ZnNc* to C_{60} was confirmed by the growth of the absorption bands of ZnNc$^{\bullet+}$ at 970 nm and $C_{60}^{\bullet-}$ at 1080 nm, accompanied by a concurrent decay of the absorption band of ^{3}ZnNc* at 600 and 770 nm (Fig. 13b). A similar ET process was observed in the case of C_{70} with ^{3}ZnNc* (Fig. 13c), in which the growth of the ab-

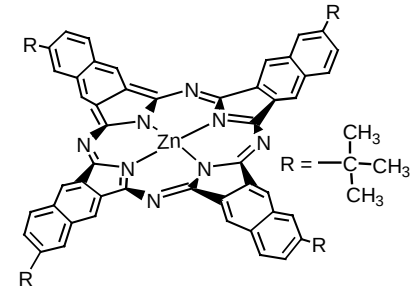

Fig. 12. Zinc tetra-*t*-butylnaphthalocyanine.

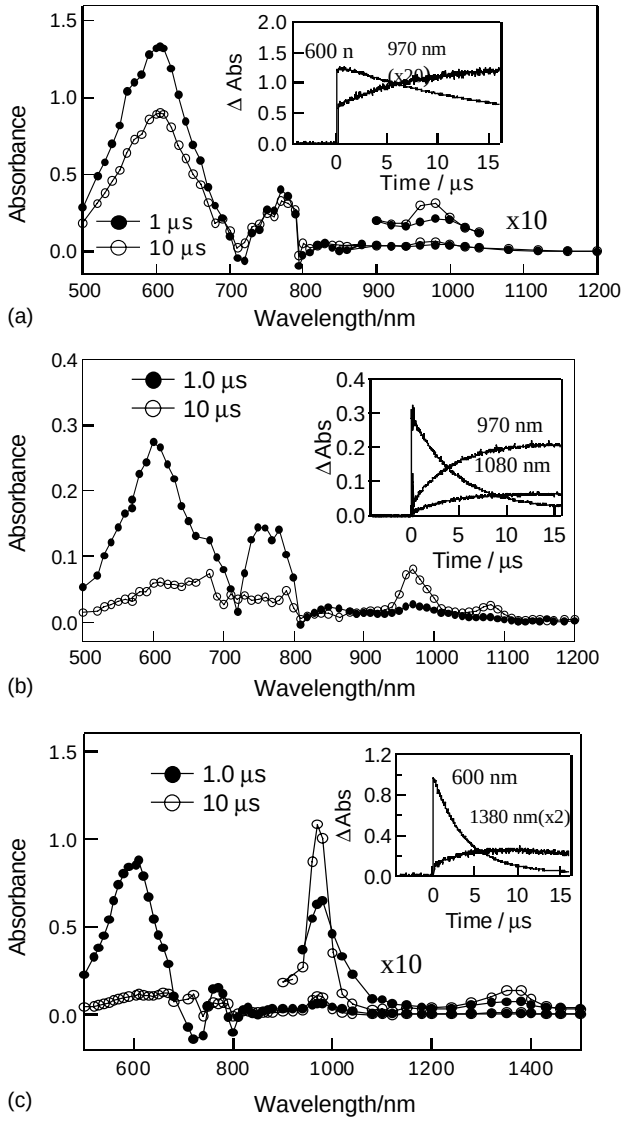

Fig. 13. Transient absorption spectra obtained by 650 nm laser light of ZnNc (0.1 mM): (a) in the absence and (b) in the presence of C_{60} (0.1 mM) and (c) C_{70} (0.1 mM) in Ar-saturated BN. Inset: time profiles.

sorption bands of $ZnNc^{\bullet+}$ (970 nm) and $C_{70}^{\bullet-}$ (1380 nm) was accompanied by the decay of $^3ZnNc^*$ (600 nm). These findings indicate that ET occurs from $^3ZnNc^*$ to C_{60}/C_{70}, with a small contribution from photoionization in polar solvents. The weaker absorption intensity of $C_{70}^{\bullet-}$ at 1380 nm (Fig. 13c) compared to that of $C_{60}^{\bullet-}$ at 1080 nm (Fig. 13b) was attributed to the smaller extinction coefficient (ε) value of $C_{70}^{\bullet-}$ compared to that of $C_{60}^{\bullet-}$. The second-order quenching rate constants (k_q) for ET from $^3ZnNc^*$ to C_{60}/C_{70} were evaluated. It was found that the k_q value for the $^3ZnNc^*$–C_{60} system ($1.45 \times 10^9\ M^{-1}\ s^{-1}$) is much higher compared to that of the $^3ZnNc^*$–C_{70} system ($1.3 \times 10^8\ M^{-1}\ s^{-1}$).

Summarizing the results of intermolecular ET of the C_{60}/C_{70}–MP (MTPP/Chl/MPc/MNc) systems, the following conclusions were drawn:

(i) By changing the excitation wavelength and concentration, it was possible to change the ET routes from (a) $^3MP^*$ to C_{60}/C_{70} and (b) MP to $^3C_{60}{}^*/^3C_{70}{}^*$. The Φ_{et} values of route (b) are usually higher than those of route (a) in polar solvents.
(ii) In all cases, the Φ_{et} values of ZnP–C_{60}/C_{70} systems are significantly higher compared to H_2P–C_{60}/C_{70} in polar solvents.
(iii) In the case of MOEP, the observed Φ_{et} values of M = Pd, Zn, and Mg are larger than those of Co, Ni, and Cu for $^3C_{60}{}^*$.
(iv) Chls have high electron donor abilities, similar to ZnTPP and MgOEP.
(v) (Ti=O)Pc shows a reactivity quite different from others such as (V=O)OEP.
(vi) MP, MPc and C_{60}/C_{70} absorbing wide visible region may be useful for applications such as photosynthetic solar energy conversion. For this purpose, the most important observation is the similar electron acceptor ability of $C_{70}/^3C_{70}{}^*$ to $C_{60}/^3C_{60}{}^*$, which suggests that it is unnecessary to rigorously remove C_{70} from the crude samples of C_{60}.

3. Photoinduced electron transfer in supramolecular fullerene–porphyrin/phthalocyanines systems

Supramolecular systems composed of porphyrin and fullerene moieties have received much attention from researchers in recent years [73–82]. These systems are composed of porphyrin and fullerene derivatives functionalized in such a way that the two entities are able to diffuse together and reversibly bind in solution. The modes of binding most often employed include π–π interactions, electrostatic attraction, hydrogen bonding, and axial ligation via a nitrogen-based ligand to the metal center of the metalloporphyrin.

The self-assembled donor–acceptor systems offer several advantages over intermolecular systems. First, the relative orientation of the donor and acceptor can be controlled, in some cases. This is quite important, since ET rates are dependent upon orbital overlap and distance between the donor and acceptor moieties. Second, for intermolecular systems, ET is a diffusion-controlled process, while for supramolecular systems this process is only partially governed by diffusion rates, but also by binding strength and concentration. Also, for intermolecular systems, the entity that is excited usually has enough time to undergo the ISC process from the singlet excited state to the triplet excited state before colliding with a donor or acceptor. Therefore, most intermolecular systems undergo ET via the triplet excited state. However, for self-assembled systems, in which the conditions have been properly adjusted so that a sufficient amount (>99%) of complexed donor–acceptors are present in solution, the excited species usually do not have enough time to undergo the ISC process. Therefore, most self-assembled systems undergo ET from the short-lived singlet excited state. Third, since the binding of the donor–acceptor complex is reversible in nature, after ET occurs, the individual charge-separated species ($D^{\bullet+}$ and $A^{\bullet-}$) can diffuse away from each other, creating a long-lived SSIP in a sufficiently polar medium; thus, increasing the lifetime of the CS state.

3.1. Fullerene–porphyrin systems coordinated via axial ligation

The porphyrin macrocycle is capable of binding a variety of transition metals within its central cavity, thus leaving the positions axial to the plane of the porphyrin ring available for binding with a variety of ligands. In 1999, three different research groups studied systems composed of C_{60} functionalized with a coordinating ligand capable of axially ligating to the metalloporphyrin metal center (MTPP; M = Zn and Ru) [73–81,113–115].

A system composed of a pyridine-appended C_{60} (py∼C_{60}) axially ligated to ZnTPP through the pyridine nitrogen (Fig. 14a) was studied by D'Souza and co-workers [114]. Upon complexation of py∼C_{60} to ZnTPP, (the symbol ∼ refers to a covalent bond) the optical absorption spectrum experienced a red shift of the Soret band. A control experiment using a phenyl-appended C_{60} derivative exhibited no such spectral shift, confirming that axial coordination occurs through the pyridine nitrogen, but not through the pyrrolidine nitrogen. The binding constant (K) was obtained from absorption spectral data using the Scatchard method to be $7337\ M^{-1}$ for ZnTPP←py∼C_{60}, (the symbol ← refers to coordination bond). The estimated ET rate for the system from steady-state fluorescence quenching studies was found to be $(2.4 \pm 0.3) \times 10^8\ s^{-1}$, which is smaller than those of covalently bonded ZnTPP∼C_{60} dyads [50–52].

Two similar systems composed of a pyridine-appended C_{60} molecule axially ligated to MTPP (M = Zn and Ru in Fig. 14b) were studied by Pasimeni and co-workers [72,73]. The Ru based system exhibited photochemistry that was strongly solvent-dependent in nature. In a nonpolar solvent

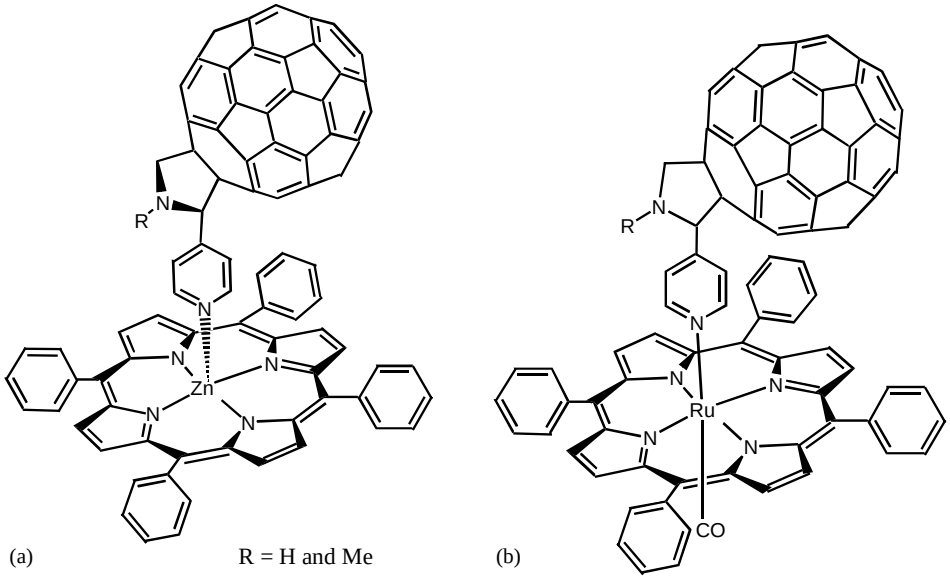

Fig. 14. Structure of the (a) zinc tetraphenylporphyrin:(4-pyridyl)fulleropyrrolidine and (b) ruthenium tetraphenylporphyrin:(4-pyridyl)fulleropyrrolidine dyads.

such as toluene, the excitation of the RuTPP leads primarily to the formation of ^{3}RuTPP* through a rapid ISC process following the initial excitation. After employing a 532 nm laser light pulse, the transient absorption spectrum of the dyad (RuTPP←py∼C_{60}) at 85 ps exhibited a broad absorption maximum at 710 nm with a shoulder at 820 nm. The 710 nm feature corresponds to the absorption of the $^3C_{60}$* moiety. These findings suggest intramolecular energy transfer from ^{3}RuTPP* to the py∼C_{60} moiety. The dyad had a Φ_{ISC} value of 0.65 and lifetime of 43 μs.

$$[^3\text{RuTPP}^* \leftarrow \text{py} \sim \text{C}_{60}] \rightarrow [\text{RuTPP} \leftarrow {}^3\text{py} \sim \text{C}_{60}^*] \quad (6)$$

Upon changing to more polar solvents such as BN or dichloromethane, a marked change in the photochemical behavior of the system was observed. Upon irradiation with a laser light pulse at 532 nm of the dyad in BN, the Q-bands were bleached out, and a set of new peaks at 565, 610, and 670 nm were observed in the transient absorption spectrum. These peaks correspond to RuTPP$^{\bullet+}$. Also, a peak at 1010 nm appeared in the near-IR region of the spectrum, which decayed after about 50 μs. This peak corresponds to the formation of $C_{60}^{\bullet-}$. These data support the mechanism of ET via ^{3}RuTPP* in BN.

$$[^3\text{RuTPP}^* \leftarrow \text{py} \sim \text{C}_{60}] \rightarrow [\text{RuTPP}^{\bullet+} \leftarrow \text{py} \sim \text{C}_{60}^{\bullet-}] \quad (7)$$

The same experiment in dichloromethane yielded different results. The data are consistent with the ET mechanism and the formation of the radical ion-pair, as was observed in BN; however, the CR process occurred much faster (<4 ns). This is attributed to the ability of BN to compete with the pyridine ligand for the axial coordination site. This promotes bond cleavage of the Ru←pyridine bond, thus creating a SSIP, which slows down the CR process. However, in solvents not capable of axially ligating to the Ru metal center, this process does not occur and hence leads to a very fast charge recombination [73].

A similar system was studied for ZnTPP and C_{60} with pyridine axially ligated to the Zn atom. Transient absorption spectra recorded in toluene and dichloromethane after a laser light flash (532 nm) yielded similar results as compared to the ruthenium-based dyad. Broad absorptions appeared at 715, 960, and 1010 nm, corresponding to ZnTPP$^{\bullet+}$ and $C_{60}^{\bullet-}$, respectively [74]. These data indicate that the system undergoes ET from ^{1}ZnTPP* to C_{60}.

$$[^1\text{ZnTPP}^* \leftarrow \text{py} \sim \text{C}_{60}] \rightarrow [\text{ZnTPP}^{\bullet+} \leftarrow \text{py} \sim \text{C}_{60}^{\bullet-}] \quad (8)$$

Investigation of the same dyad system in BN using transient absorption methods revealed the formation of a broad absorption around 730 and 1010 nm, in which the latter corresponds to the formation $C_{60}^{\bullet-}$. However, the formation $C_{60}^{\bullet-}$ was revealed via two routes; a slow component was due to ET from ^{3}ZnTPP*, while the fast component was due to ET from ^{1}ZnTPP*. This can be rationalized by considering that BN is a coordinating solvent capable of competing with C_{60} pyridine for the axial coordination site. Thus, both inter- and intramolecular ET mechanisms are possible pathways.

Our research groups recently performed a systematic study on donor–acceptor systems composed of C_{60} bearing nitrogen-based ligands (*o*-pyridyl, *m*-pyridyl, *p*-pyridyl, *N*-phenyl imidazole) axially ligated to ZnTPP (Fig. 15) [79]. UV-Vis spectral data were used to determine the binding constants (K) for each C_{60} derivative with ZnTPP. The trend observed for the K values was: *o*-pyridyl ≪ *m*-pyridyl ≈ *p*-pyridyl ≪ *N*-phenyl imidazole. Thermodynamic param-

Table 9
Formation constant, K and thermodynamic parameters for self-assembled zinc tetraphenylporphyrin–fulleropyrrolidine conjugates in *o*-DCB

Ligand[a]	K[b] (M^{-1})	ΔG ($kJ\,mol^{-1}$)	ΔH ($kJ\,mol^{-1}$)	ΔS ($J\,K^{-1}\,mol^{-1}$)
Pyridine	7750	−22.1	−27.3	−17.1
N-Phenyl imidazole	18620	−24.0	−32.4	−28.2
1	[c]	–	–	–
2[b]	7740	−22.1	−26.1	−12.3
3	7660	−22.1	−26.7	−15.4
4	7170	−22.0	−26.9	−16.5
5	16110	−23.6	−31.9	−28.1

[a] For abbreviations see Fig. 15.
[b] At 298 K.
[c] No appreciable binding was observed.

eters for these systems were also evaluated, as summarized in Table 9. These data suggested that both enthalpy and entropy changes contribute to the overall free energy change for the self-assembly of the systems studied.

X-ray structural and ab initio computational studies on of the supramolecules involving *p*-pyridyl derivatized fulleropyrrolidine and ZnTPP were also performed [116]. In the studied solid state structure, the zinc-to-axially coordinated pyridyl nitrogen distance was found to be 2.158 Å which is compatible with a 2.075 Å average distance of the porphyrin ring Zn–N bonds. Importantly, the center-to-center distance between the porphyrin zinc ion and fullerene was ca. 9.53 Å. Additional intermolecular interactions between the zinc porphyrin and the C_{60} unit that is not directly coordinated to the zinc were also observed in the crystal packing.

Steady-state fluorescence experiments were performed in *o*-dichlorobenzene (*o*-DCB) on the dyad systems. Stern–Volmer plots were used to calculate the bimolecular quenching constants (k_q^S). These values were found to be 2–3 orders of magnitude greater than would be expected for a diffusion-controlled process. In BN, a coordinating solvent, the quenching constant decreases significantly, probably due to the competition between the solvent and the C_{60} derivative for the axial coordination site.

Time-resolved fluorescence experiments showed a similar trend to that of the steady-state data. Upon addition of the C_{60}-coordinating derivatives to a solution containing ZnTPP the quenching of ^{1}ZnTPP* was accelerated (monitored at 600 nm). Upon addition of **3**, the CS rate constant (k_{cs}) and quantum yield (Φ_{cs}) increased only slightly. However, for **5**, these values increased greatly (Table 10). Also, the quenching process was found to consist of both a slow and a fast process, probably due to bound and unbound species present in solution.

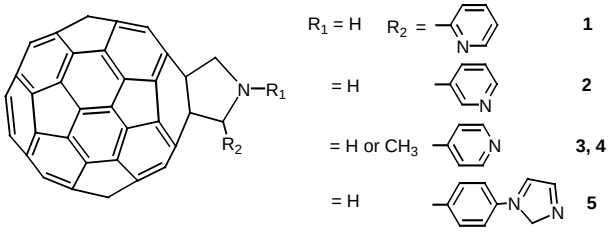

Fig. 15. Structure of the fullerene derivatives functionalized to bear pyridine and imidazole ligands used to complex with zinc porphyrin.

Time-resolved transient absorption spectra were recorded to confirm the mechanism of CS for the studied dyads. Transient absorption spectra of **5** with ZnTPP in *o*-DCB (530 nm laser excitation) exhibit a peak at 1000 nm after 0.01 μs, which is attributed to $C_{60}^{\bullet-}$. This peak then decays very rapidly ($<10^8\ s^{-1}$), indicating that CS occurs from ^{1}ZnTPP* and decays very rapidly under these experimental conditions. The transient absorption spectra in BN showed very different features. Here, the absorption bands of ^{3}ZnTPP* at 840 and 700 nm decay quickly and the rise of the transient absorption band at 1020 nm was attributed to $C_{60}^{\bullet-}$. These data indicate that, for the dyad system composed of **5** and ZnTPP in BN, the ET process occurs mainly from the triplet excited state (^{3}ZnTPP*), with an estimated ET rate constant (k_{et}^T) of $2.5 \times 10^7\ M^{-1}\ s^{-1}$. The different photochemical pathways are shown in the energy diagrams in Fig. 16.

Table 10
Fluorescence lifetimes (τ), CS rate constants ($k_{CS}^{singlet}$) and quantum yields ($\Phi_{CS}^{singlet}$) for ZnTPP←fulleropyrrolidine supramolecular dyads in *o*-DCB

Compound[a]	Solvent	τ_f (ns) (fraction %)	$k_{CS}^{singlet}$ (s^{-1})[b]	$\Phi_{CS}^{singlet}$ [c]
ZnTPP	DCB	2.10 (100)	–	–
ZnTPP←**3** (1:1)	DCB	1.88 (100)	5.6×10^7	0.10
ZnTPP←**3** (1:6)	DCB	1.85 (100)	6.3×10^7	0.12
ZnTPP←**5** (1:1)	DCB	0.058 (30)	1.7×10^{10} [d]	0.97[d]
		2.00 (70)	5.3×10^9 [e]	0.61[e]
ZnTPP←**5** (1:6)	DCB	0.058 (50)	1.7×10^{10} [d]	0.97[d]
		2.00 (50)	8.6×10^9 [e]	0.84[e]

[a] For abbreviations see Fig. 15.
[b] $k_{CS}^{singlet} = (1/\tau_f)_{sample} - (1/\tau_f)_{ref}$.
[c] $\Phi_{cs}^{singlet} = [(1/\tau_f)_{sample} - (1/\tau_f)_{ref}]/(1/\tau_f)_{sample}$.
[d] From the fast decay.
[e] Average value.

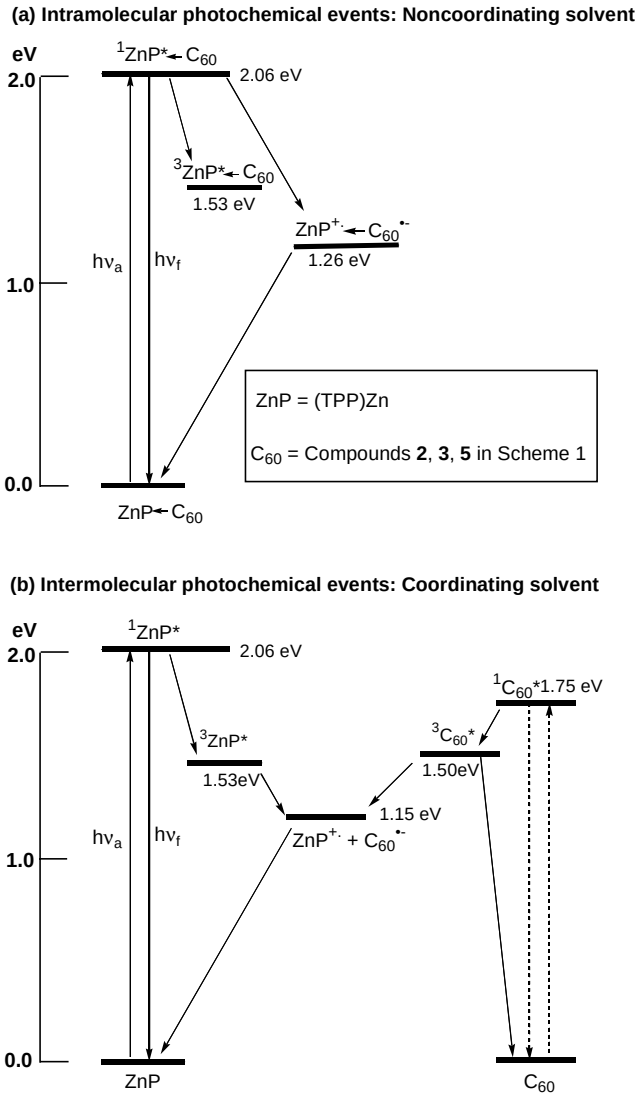

Fig. 16. Energy level diagram showing (a) intramolecular photochemical events of ZnTPP←fulleropyrrolidine dyads and (b) intermolecular photochemical events of ZnTPP—fulleropyrrolidine mixture.

Our research groups recently prepared and studied a supramolecular dyad system composed of an imidazole-appended C_{60} (**5**), which axially coordinates via the imidazole nitrogen to the central metal of ZnNc (Fig. 17) [113]. UV-Vis spectral data were used to confirm the formation of the self-assembled dyad system. Upon addition of **5** to a solution containing ZnNc (toluene), the absorbance band at 767 nm exhibited diminished intensity, and isosbestic points appeared at 675, 717, 752, and 791 nm. The *K* value for the dyad in toluene solution was determined to be $6.2 \times 10^4\ M^{-1}$ by the Scatchard method. This value is an order of magnitude larger than that of the counterpart ZnTPP dyad system.

Steady-state fluorescence experiments were performed on the self-assembled dyad system. Upon addition of **5** to a solution containing ZnNc (toluene or *o*-DCB), the emission bands at 781 and 812(sh) nm were gradually quenched to

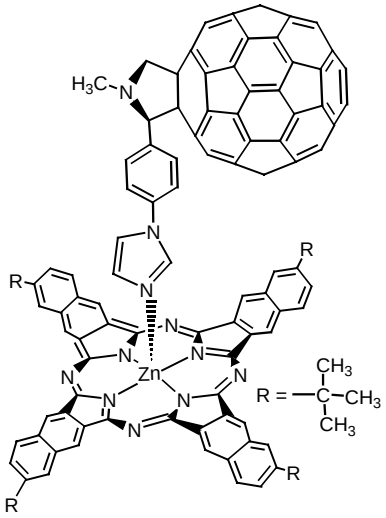

Fig. 17. Structure of the naphthalocyanine:fullerene conjugate self-assembled via axial ligation.

about 30% of the original intensity. Also, the emission band at 781 nm experiences a 3 nm blue shift compared to the original uncoordinated ZnNc. Stern–Volmer plots were used to determine the quenching constant for the dyad system. This value was determined to be four orders of magnitude larger than what would be expected for a diffusion-controlled process. This indicates that an intramolecular quenching process is the predominant quenching pathway for the dyad system.

Time-resolved fluorescence spectral studies were performed on the dyad system. The excited state of pure ZnNc had a lifetime of 2.42 ns. Upon addition of **5** to form the complex (**5**→ZnNc) (toluene) the excited state decayed bi-exponentially, having both fast and slow components. The fast component had a lifetime of around 71 ps, while the slow component had a lifetime of around 2.14 ns. The slow component lifetime was similar to that obtained for uncomplexed ZnNc. The short-lived nature of the excited state of ZnNc in the complex (**5**→ZnNc) suggests quenching via ET from the singlet excited state of ZnNc (^{1}ZnNc*). The k_{cs} value was determined to be $1.4 \times 10^{10}\ s^{-1}$, with a Φ_{cs} value of 0.97 for the process (toluene).

Picosecond transient absorption spectra were obtained in order to determine the nature of the excited state photochemical reactions in this time domain. Upon excitation of the dyad with 388 nm laser light, new bands appeared at 710 and 985 nm in the time region of 10–200 ps (Fig. 18). These bands were attributed to the formation of ZnNc$^{\bullet+}$. The band expected at 1000 nm representing **5**$^{\bullet-}$ was not observed, probably due to masking by the intense band at 985 nm. The k_{cs} value for the dyad was evaluated to be $1.4 \times 10^{10}\ s^{-1}$, which is in agreement with the value determined by fluorescence lifetime measurements, while the k_{cr} value was evaluated to be $8.5 \times 10^8\ s^{-1}$.

Nanosecond transient absorption spectra were also obtained for the self-assembled dyad. Upon excitation of the dyad (**5**→ZnNc) with 532 nm laser light, intense absorption

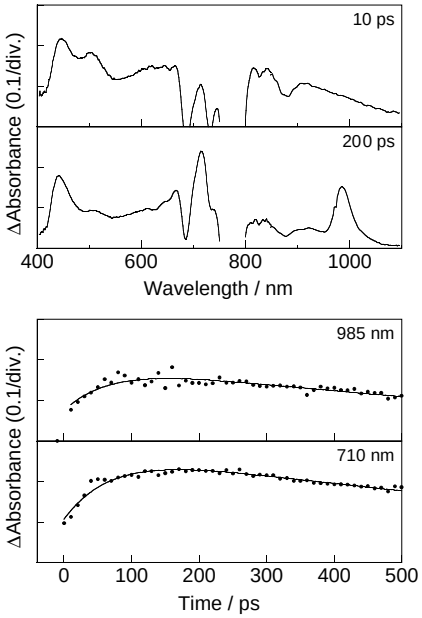

Fig. 18. Upper panels: transient absorption spectra of ZnNc (0.03 mM) in the presence of C_{60}Im (0.3 mM) in toluene. Lower panels: time profiles at 985 and 710 nm [113].

bands were observed between 600 and 700 nm after 100 ns, corresponding to ^{3}ZnNc* and ^{3}**5***. After 10 ns, absorption bands were observed in the region of 960–1000 nm, corresponding to the formation of the radical ion pair ($\mathbf{5}^{\bullet-}\rightarrow$ZnNc$^{\bullet+}$). These absorption bands show quick rise-decay behavior, indicating a rapid CR process.

The transient absorption spectra in coordinating solvents such as BN were quite different. Upon excitation of the dyad with 650 nm laser light, the spectra exhibited bands at 600 and 750 nm, which were attributed to appreciable population of ^{3}ZnNc* and ^{3}**5***. These absorption bands of the triplet states decay, accompanied by the rise of the absorption bands in the 960–1000 nm region, which were attributed to the formation of the radical ion pairs, ZnNc$^{\bullet+}$ and $\mathbf{5}^{\bullet-}$. These data suggest that in a coordinating solvent the ET process takes place from ^{3}ZnNc* to **5**. The bimolecular ET rate constant (k_{et}) was evaluated to be $1.3 \times 10^8\,M^{-1}\,s^{-1}$, while the back ET rate constant (k_{bet}) was determined to be $3.6 \times 10^9\,M^{-1}\,s^{-1}$.

Schuster and co-workers [117] also developed and studied a dyad system composed of a pyridine-appended C_{60} that axially ligates to the central metal of ZnTPP with a linear geometry (Fig. 19). Therefore, the donor–acceptor distance in the dyad is greatly increased. Due to the increased electron density around the pyridine nitrogen, it was shown to have a greater capacity to bind to the zinc central metal. This was confirmed by steady state fluorescence quenching experiments where the K value was determined to be $7.4 \times 10^4\,M^{-1}$ in *o*-DCB. Also, these experiments show that fluorescence quenching occurred quite efficiently in both polar and nonpolar solvents.

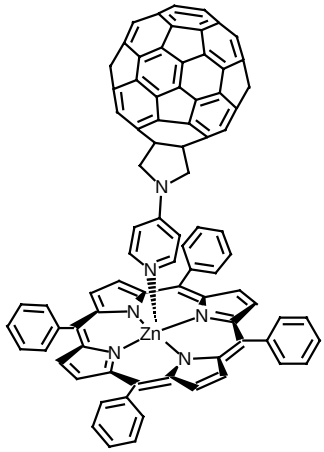

Fig. 19. Structure of the investigated zinc porphyrin–fullerene dyad.

Nierengarten and co-workers studied a similar dyad [115]. This dyad was composed of a pyridine-appended C_{60} molecule (py∼C_{60}) synthesized by Bingel addition to the fullerene, which can axially coordinate to ZnTPP via the central metal atom (Fig. 20a). Steady state fluorescence was used to arrive at an association constant of $K_a = 3000 \pm 400\,l\,M^{-1}$ for the complex in toluene. Upon excitation of ZnTPP in the presence of py∼C_{60}, the fluorescence of ZnTPP was quenched. This quenching was rationalized to occur as a result of the CS process from ZnTPP to py∼C_{60}, owing to the very large rate constant observed ($k_{CS} > 5 \times 10^{10}\,s^{-1}$). Also, the nonpolar nature of the solvent contributes to the observation of the EN process, since the CS state is unstable in nonpolar media relative to polar solvent media. EN processes in the system were found to have a slow and fast component. The fast component was thought to exist as a result of singlet–singlet energy transfer in the associated complex, while the slow component occurs via triplet–triplet energy transfer for the unassociated complex [115].

Other coordinated porphyrin–fullerene dyad systems have been developed to increase the donor–acceptor distance and thereby probe its effect on energy or electron transfer events. Guldi, Hirsch, and coworkers [74] developed a dyad system composed of a heterofullerene ($C_{59}N$) appended with a pyridine moiety capable of axial ligation to the central metal of a zinc tetrakis(*p-tert*-butylphenyl)porphyrin entity (ZnTBPP) (Fig. 20b). In this system the pyridine linkage to $C_{59}N$ has an almost linear geometry, and thus the donor–acceptor distance is greatly increased relative to those systems previously discussed in this review.

Steady-state fluorescence data were used to determine the K value of the dyad (ZnTBPP←py∼$C_{59}N$), which was around $10{,}000\,M^{-1}$ in non-coordinating solvents (toluene, *o*-DCB). Upon addition of increasing amounts of the $C_{59}N$ to ZnTBPP, the fluorescence of ZnTBPP was steadily quenched. Time-resolved fluorescence decay experiments were performed to probe the nature of the dyad

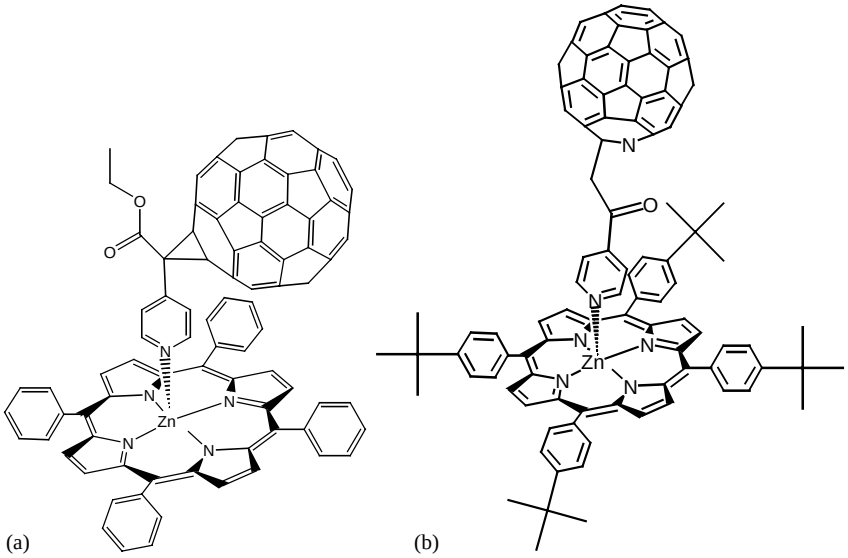

Fig. 20. Structure of axially coordinated zinc porphyrin:pyridine-appended fullerene conjugates.

excited state. Upon laser excitation at 337 nm, the decay profile displayed both a short-lived and long-lived component, with lifetimes of 0.15 and 1.9 ns, respectively. These experiments also revealed emission of $C_{59}N$ at around 825 nm, indicating that the excited state of $C_{59}N$ is being populated.

Transient absorption experiments were performed to determine the nature of the photochemical reactions for the studied dyad. Upon addition of the axially ligating py∼$C_{59}N$ to ZnTBPP in toluene and laser light excitation at 535 nm, ^{1}ZnTBPP* decayed very rapidly, with a lifetime of about 2.3 ns. Peaks appeared in the transient spectra at 735 and 940 nm. This indicates that, due to the rapid decay of the excited state, the deactivation takes place from ^{1}ZnTBPP* and populates $C_{59}N$ via a singlet–singlet energy transfer mechanism. The $^1C_{59}N^*$ state subsequently decayed to $^3C_{59}N^*$ via the ISC process with a rate constant of $1.0 \times 10^9\ s^{-1}$ which then decays further to the ground state, with a lifetime of 15 μs.

However, in a more polar solvent such as *o*-DCB, the transient absorption spectra of the dyad were quite different. After laser light excitation of ZnTBPP (18 ps), ^{1}ZnTBPP* decays, rapidly revealing peaks at 640 and 1020 nm, which correspond to $ZnTBPP^{\bullet+}$ and $C_{59}N^{\bullet-}$, respectively. These data indicate that the photoinduced ET is the predominant photochemical reaction process in polar medium.

3.2. Two-point binding supramolecular triads with electron donor

Our research groups recently prepared and studied a novel triad system composed of a zinc porphyrin appended with hydrogen-bonding groups such as either a carboxylic acid or an amide group (ZnTPP∼COOH or ZnTPP∼NH_2) and a C_{60} molecule appended with a pyridine group and a *N*,*N*-dimethylaniline (DMA) group acting as a secondary electron donor (C_{60}∼DMA) (Fig. 21) [118]. The triad system is self-assembled via a "two-point" binding motif, where the pyridine group on the C_{60} axially ligates to the central metal of the zinc porphyrin, while the nitrogen of the fulleropyrrolidine ring hydrogen bonds with the hydrogen-bonding group attached to ZnTPP, either ZnTPP∼COOH or ZnTPP∼$CONH_2$.

UV-Vis, ^{1}H NMR, and ab initio B3LYP/3–21G(*) computational studies were used to verify the integrity of the self-assembled triads. Upon addition of C_{60}∼DMA to a solution containing either ZnTPP∼COOH or ZnTPP∼$CONH_2$,

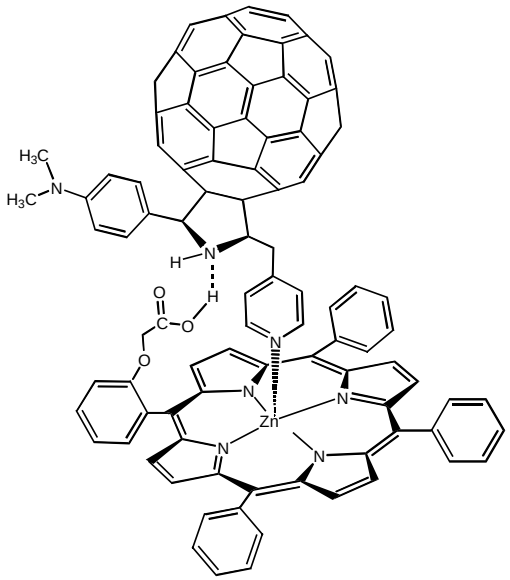

Fig. 21. Structure of the zinc porphyrin–fullerene-dimethylaminophenyl supramolecular triad bound by "two-point" hydrogen bonding-coordinate bonding.

a characteristic decrease and red shift of the Soret band were observed. Also, upon addition of either ZnTPP∼COOH or ZnTPP∼NH_2 to a solution of C_{60}∼DMA, the pyridine and fullerpyrrolidine protons experienced an upfield shift caused by interaction with the ring current of the porphyrin ring, while the amide and carboxylic acid protons experienced a downfield shift due to hydrogen bonding interactions. These results clearly indicated the formation of the supramolecular triad system via the "two-point" binding motif. The K values for the triads C_{60}∼DMA→ZnTPP∼COOH and C_{60}∼DMA→ZnTPP∼$CONH_2$ were arrived at via Scatchard plots and were determined to be 10×10^4 and $3.1 \times 10^4\ M^{-1}$, respectively.

Steady-state fluorescence experiments were carried out on the supramolecular triad systems. Upon addition of C_{60}∼DMA to a solution containing either ZnTPP∼COOH or ZnTPP∼NH_2 in *o*-DCB, the fluorescence emission intensity of the ZnTPP moiety was quenched to about 30% of its original value. Also, a weak band at 710 nm, corresponding to the emission of C_{60}, was observed. Compared with the results of a control experiment where C_{60}∼DMA was added to ZnTPP, the observed fluorescence showed that the amount of C_{60}∼DMA needed to quench emission by the same extent as with ZnTPP∼COOH or ZnTPP∼NH_2 was about 25% less. These data indicate that the efficiency of the charge separation process is increased as a result of the stronger "two-point" binding.

Time-resolved fluorescence emission experiments were also performed on the self-assembled triad systems. The singlet excited state lifetimes of ZnTPP, ZnTPP∼COOH, and ZnTPP∼$CONH_2$ were determined to be 1.92, 2.35, 1.97 ns, respectively. Upon complexation with C_{60}∼DMA, fast fluorescence decay was observed, indicating that the CS process from the singlet excited states occurred. The fluorescence decay was found to be more efficient for the "two-point" bound systems as compared with the singly bound counterpart. These data indicate that the DMA moiety acts as a secondary electron donor and accelerates the CS process (Table 11).

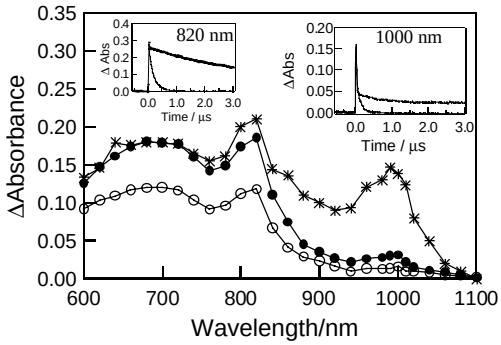

Fig. 22. Transient absorption spectra obtained by 532 nm laser light of C_{60}NDMA→ZnTPP∼$CONH_2$ (0.1 mM, 1:1 eq.) in *o*-DCB: (✱) 0.01 μs, (●) 0.25 μs and (○) 2.5 μs. Inset: time profiles of the 820 and 1000 nm bands [118].

Transient absorption spectra were obtained to determine the nature of the excited state photochemical reactions for the self-assembled dyads (Fig. 22). The transient absorption spectra of C_{60}∼DMA:ZnTPP∼NH_2 obtained after 532 nm laser light flash after 0.01 μs exhibited bands at 700, 870, and 1000 nm corresponding to $^3C_{60}{}^*$, ^{3}ZnTPP∼$NH_2{}^*$, and $C_{60}{}^{\bullet-}$, respectively. The $C_{60}{}^{\bullet-}$ band at 1000 nm was still observed in the transient absorption spectra after 0.25 μs. This indicates that the DMA group aids in the stabilization of the CS state. The CS state exhibited both a fast ($k = 3.1 \times 10^7\ s^{-1}$) and slow ($k = 3.5 \times 10^5\ s^{-1}$) component for the CR process.

The relatively strong binding in the "two-point" bound triad system is thought to play a role in the increased stabilization of the CS state. A comparison of the ratio k_{CS}/k_{CR}, which reflects the ET efficiency, shows that as the K values increase for the "two-point" bound system, so does k_{CS}/k_{CR}. This indicates that for the more strongly bound systems the efficiency of the ET process increases. Also, the DMA group is thought to play a role in slowing down CR and thereby increasing the lifetime of the CS state for the triad system. Since the E_{ox} value of the DMA group is relatively low,

Table 11
Binding constants (K), fluorescence lifetimes (τ_f)[a], CS rate constants ($k_{CS}^{singlet}$), quantum yields ($\Phi_{CS}^{singlet}$) and CR rate constants (k_{CR}) for *N*,*N*-dimethylaminophenyl-zinc porphyrin←C_{60} triads in *o*-DCB

Complex	K (M^{-1})	τ_f[a] (fraction %)	$k_{CS}^{singlet}$ (s^{-1})	$\Phi_{CS}^{singlet}$[b]	k_{CR} (s^{-1})	k_{CS}/k_{CR}
C_{60}py→ZnTPP	0.77×10^4	1.85 ns (100)	6.3×10^7	0.12	3.0×10^7	2
C_{60}∼DMA→ZnTPP	0.78×10^4	71 ps (27) 2.03 ns (73)	1.4×10^{10}[b] 1.5×10^8[c]	0.97[b] 0.22[c]	3.4×10^7	4
C_{60}∼DMA→ZnTPP∼$CONH_2$	3.1×10^4	69 ps (81) 1.60 ns (19)	1.4×10^{10}[b] 1.8×10^9[c]	0.98[b] 0.77[c]	3.1×10^7	58
C_{60}∼DMA→ZnTPP∼COOH	10×10^4	8 ps (75) 2.28 ns (25)	1.3×10^{11}[b] 1.8×10^9[c]	0.99[b] 0.67[c]	2.3×10^7	43

[a] The singlet lifetimes of ZnTPP, ZnTPP–$CONH_2$, ZnTPP–COOH in deareated *o*-DCB were found to be 1.92, 1.97, and 2.35 ns (mono-exponential decay), respectively.
[b] From the fast decay.
[c] Average values.

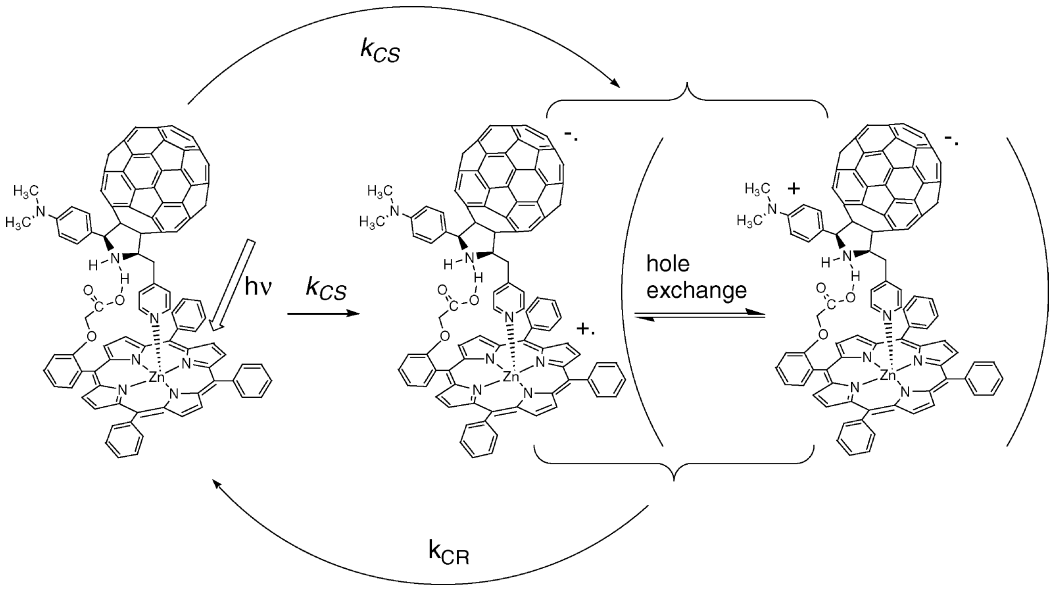

Fig. 23. Proposed mechanism of the photochemical charge stabilization in the self-assembled DMA∼C_{60}Py→ZnP∼COOH triad.

after the initial charge separation generating $ZnTPP^{\bullet+}$ and $C_{60}^{\bullet-}$, the DMA group donates an electron to $ZnTPP^{\bullet+}$. Thus, a hole shift occurs from $ZnTPP^{\bullet+}$ to the DMA group, which is stable owing to the irreversible nature of the DMA oxidation, as shown in Fig. 23. These processes are thought to be the mechanism of the slow CR that is observed.

3.3. Fullerene–porphyrin coordinated systems: control over distance and orientation

The relative distance and orientation between an electron donor and acceptor in a dyad-type system greatly affect electron transfer rates and lifetimes. Recently, researchers have been developing dyad systems, where the distance and orientation of the donor and acceptor can be controlled, thereby allowing for their effects on the ET processes to be studied [33,36,48–52]. In this regard, we recently prepared an exotic dyad system composed of ZnTPP covalently linked with C_{60} appended with a pyridine ring [119]. The pyridine ring (4-pyridyl or 3-pyridyl) on C_{60} can either exist in the bound ("tail-on") or unbound ("tail-off") form by axial ligation to the ZnTPP (Fig. 24). The relative donor–acceptor proximity was varied by adjusting temperature or the concentration of a competing ligand (3-picoline). It was observed at room temperature that the Soret bands of the studied dyads were located around 433 nm, which is close to that of a

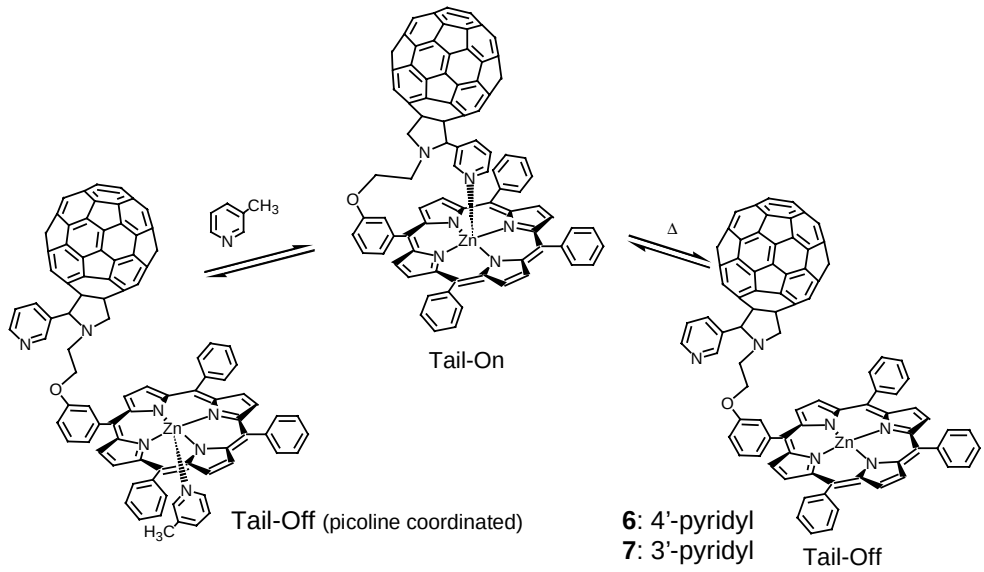

Fig. 24. Structure of zinc porphyrin–fullerene dyads utilizing 'tail-on' and 'tail-off' binding processes.

Table 12
Equilibrium constant (K) and thermodynamic parameters for the temperature-controlled 'tail-on' and 'tail-off' processes of zinc porphyrin–C_{60} dyads in *o*-DCB

Dyad[a]	K[b] (M^{-1})	ΔG (kJ mol^{-1})	ΔH (kJ mol^{-1})	ΔS (J K^{-1} mol^{-1})
7	17.29	−7.07	−19.17	−40.59
6	14.43	−6.62	−18.11	−38.52
ZnP_m∼py[c]	2.99	−2.72	−45.36	−138.6

[a] For abbreviations see Fig. 24.
[b] At 298.15 K.
[c] Represents a pyridine-appended porphyrin.

penta-coordinated ZnTPP–pyridine complex. Therefore, it was assumed that the dyads are predominantly in the "tail-on" form at room temperature. The K values for the dyads and thermodynamic parameters were determined by the Van't Hoff method using variable temperature UV-Vis spectral data. These data suggest that there are both entropic and enthalpic contributions to the overall binding process (Table 12).

Steady-state fluorescence experiments were performed on the dyads using the addition of picoline as a competing ligand to vary the amount of the "tail-on" and "tail-off" forms present in solution. Upon addition of excess picoline (10 eq.) to shift the equilibrium to the "tail-off" form, the emission intensity of the ZnTPP moiety increased by about 27%. This fluorescence emission behavior was most likely due to the increased distance between the donor and acceptor in the "tail-off" form and minor structural changes to the system.

Picosecond time-resolved fluorescence experiments were performed to investigate the nature of the excited state for the investigated dyads. In the case of the 4-pyridyl-substituted derivative, the "tail-on" form slightly accelerates the CS process. The reverse is observed for the 3-pyridyl-substituted derivative, suggesting that, in this case, the "tail-off" form facilitates structural changes that promote rapid CS process.

Nanosecond transient absorption spectra were recorded to elucidate the nature of the CS state. Bands corresponding to $^3C_{60}$*, ^{3}ZnTPP*, and $C_{60}^{\bullet -}$ appeared in the transient absorption spectra at 700, 850, and 1000 nm, respectively. The triplet bands decayed with a lifetime of around 600 ns. The decay profile exhibited both fast and slow decay components indicating that there are two types of decay processes from the CS state. This was attributed to relaxation from the long-lived triplet CS state and also from the singlet CS state. Upon addition of picoline, a peak at 1000 nm was observed, which is ascribed to $C_{60}^{\bullet -}$, confirming that the CS process occurs for the "tail-off" form of the dyads. Also, the relative intensity of the peak at 1000 nm versus the peak at 700 nm is greater for the "tail-off" form than for "tail-on" form. This indicated that the slow decay component from $^3C_{60}$* was a relatively minor pathway for the decay of the "tail-off" form of the CS state. Both the "tail-on" and "tail-off" forms undergo CS via ^{1}ZnTPP*, although this process is slightly more efficient for the "tail-off" form of the dyads studied.

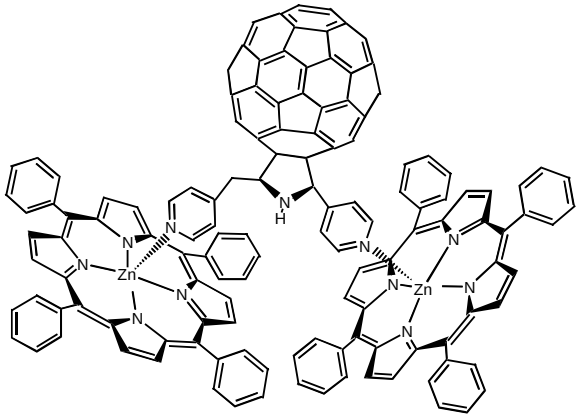

Fig. 25. Structure of the bis zinc porphyrin–fullerene triad self-assembled via axial coordination.

3.4. Fullerene–bisporphyrin coordinated triads

More recently we developed a system composed of a C_{60} unit appended with two pyridine units (C_{60}∼py_2) that axially ligate to two ZnTPP thus forming a self-assembled triad (Fig. 25) [120]. UV-Vis absorption data were used via the Scatchard method to determine the binding constant value for the system. This value was determined to be 1.45×10^4 M^{-1} which is considerably large as compared to the dyad counterpart analogue.

Steady-state fluorescence experiments were performed on the triad system. Upon addition of C_{60}∼py_2 to a solution of ZnTPP in *o*-DCB, the fluorescence was quenched to approximately 30% of its original intensity and red-shifted by 2–3 nm. The Stern–Volmer quenching constant (k_q) was determined and found to be three times larger than that of a diffusion-controlled process, suggesting that intramolecular quenching is the primary quenching pathway for the system. Also, a weak emission band at 710 nm corresponding to the singlet emission of C_{60} was observed.

Time-resolved transient absorption spectra were recorded to confirm the nature of the excited state photochemical dynamics of the system. A solution of the triad in *o*-DCB was excited by laser light at 532 nm. Bands were observed at 760 and 850 nm corresponding to $^3C_{60}$* and ^{3}ZnTPP*, respectively. Also, a weak band at 1000 nm corresponding to the $C_{60}^{\bullet -}$ was observed. The quick rise and decay of this band indicates that charge separation takes place from the singlet excited state of ZnTPP.

The absorption spectra observed in coordinating solvents such as BN were quite different. Bands were observed at 770 and 840 nm, corresponding to $^3C_{60}$* and ^{3}ZnTPP*. These bands were found to decay faster than what was observed for *o*-DCB. Also, a slow rise was observed in the 900–1100 nm region, corresponding to the formation of the $C_{60}^{\bullet -}$. These

data indicate that, in coordinating solvents, energy transfer from ^{3}ZnTPP* to C_{60} was the predominant process.

Another supramolecular triad was formed by a "covalent-coordinate" approach, where a free base porphyrin was functionalized to bear a C_{60} appended with a pyridine group (H_2TPP∼C_{60}py) capable of axial ligation with ZnTPP (Fig. 26) [80]. Steady state fluorescence experiments were performed on the supramolecular triad system. Upon addition of **6** or **7** to a solution containing ZnTPP, the two emission bands of ZnTPP at 598 and 646 nm were quenched, accompanied by the appearance of two new emission bands at 665 and 720 nm, corresponding to the emission of H_2TPP. These data indicate that an intramolecular quenching process is occurring within the self-assembled supramolecular triad system.

Picosecond time-resolved fluorescence spectral studies were performed on the covalently linked dyad systems. The short excited state lifetimes for the studied dyads (440 ps for **6** and 710 ps for **7**) indicate that an intramolecular CS process takes place from $^1H_2$TPP*. The k_{cs} values for the dyads were found to be $2.2 \times 10^9\ s^{-1}$ for **6** and $2.6 \times 10^9\ s^{-1}$ for **7**. Time-resolved fluorescence spectra were also obtained for the self-assembled triad system with ZnTPP. For the triad systems, the fluorescence quenching of ^{1}ZnTPP* was slightly accelerated; the lifetimes of ^{1}ZnTPP* of **6**:ZnTPP and **7**:ZnTPP were found to be 1.78 and 1.83 ns, respectively, while the lifetime of uncoordinated ZnTPP was 2.10 ns. Nanosecond transient absorption spectral studies were performed to determine the nature of the excited state photochemical reactions in the dyad and triad systems. The relative efficiency of intermolecular ET was evaluated by monitoring the absorbance ratio of the transient absorption bands at 700 and 1000 nm ($A_{1000\,nm}/A_{700\,nm}$). For dyad systems **6** and **7**, this ratio was determined to be 0.45 and 0.32, respectively. Upon addition of 6:1 equivalents of **6** or **7** to

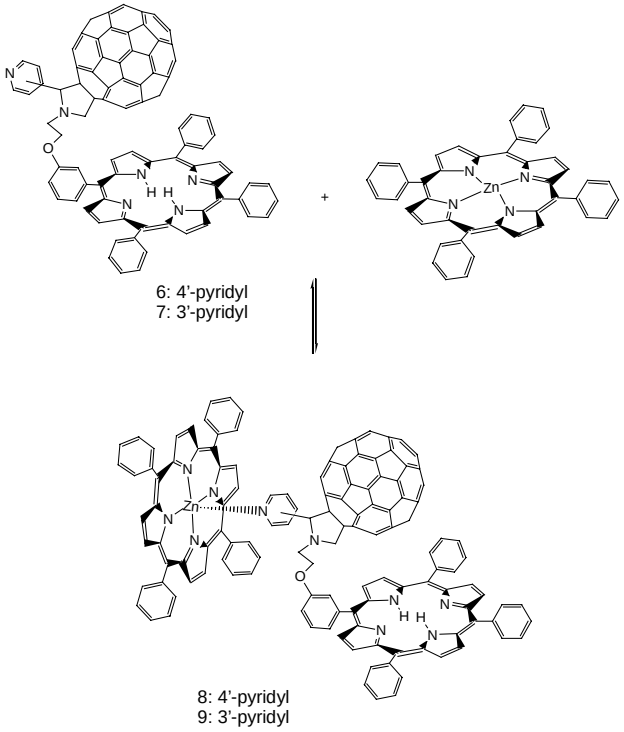

Fig. 26. Structure of H_2TPP∼C_{60}Py self-assembled to ZnTPP triads.

ZnTPP, under conditions where almost all ZnTPP is coordinated, the absorbance ratio ($A_{1000\,nm}/A_{700\,nm}$) increased to 0.50 and 0.52, respectively. These data indicate that the CS efficiency increases upon coordination of ZnTPP to the fullerpyrollidine entity of the dyads. Fig. 27 illustrates the different photochemical events in the studied triads.

In a coordinating solvent such as BN, the transient absorption spectra were quite different. Bands at 1000 and 620 nm exhibited a slow rise in the spectrum, while bands at 750

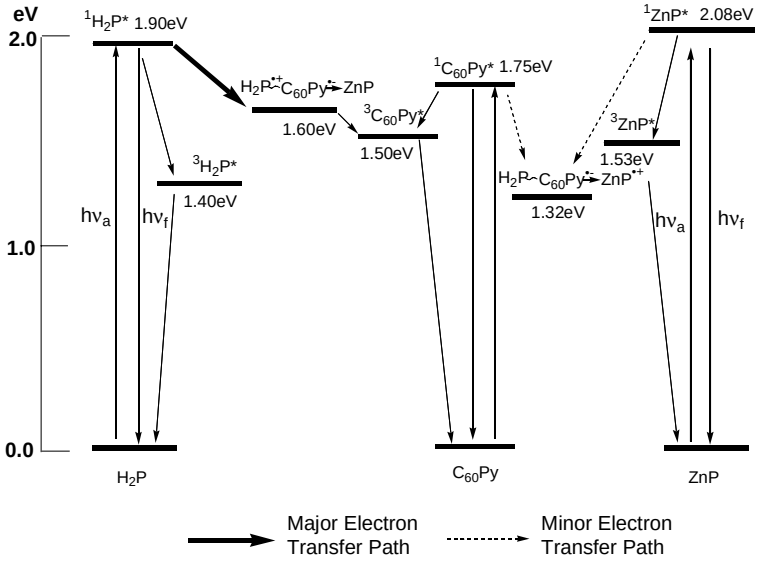

Fig. 27. Energy level diagrams showing the different photochemical events for supramolecular H_2TPP∼C_{60}Py→ZnTPP in *o*-DCB.

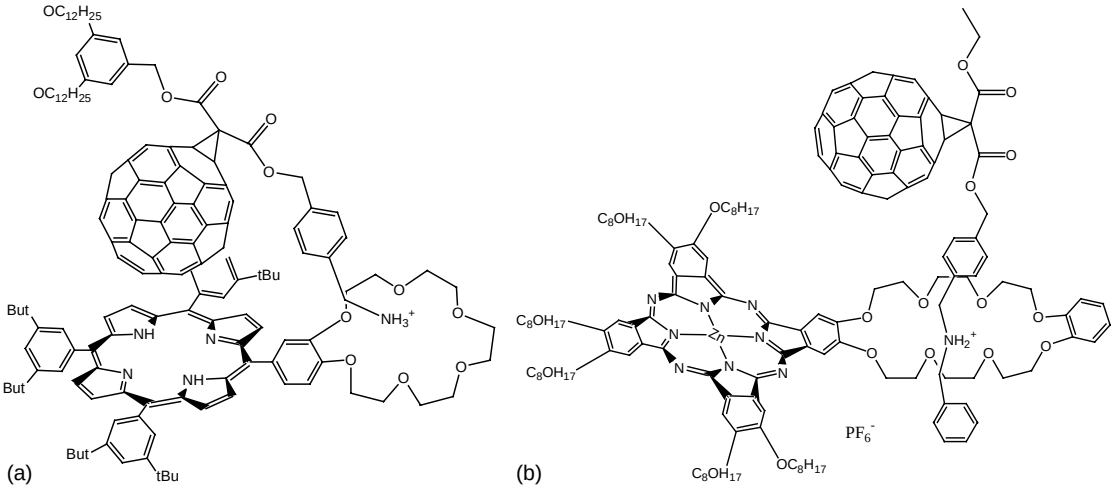

Fig. 28. Structures of crown ether complexed to fullerene bearing alkyl ammonium cation conjugate: (a) porphyrin and (b) phthalocyanine.

and 850 nm decayed at appreciable rates. These results suggest that, in coordinating solvents, intermolecular ET takes place from ^{3}ZnTPP*. The k_{et} values were determined to be 1.4×10^8 and $1.9 \times 10^8\ M^{-1}\ s^{-1}$ for triads composed of **6** and **7**, respectively.

3.5. Fullerene–porphyrin/phthalocyanine assembly systems

Recently, Nierengarten and co-workers developed a system composed of a C_{60} molecule appended with a quaternary ammonium unit and a free base porphyrin (H_2TPP) functionalized to bear a crown ether unit (Fig. 28a) [121]. The two different entities self-assemble in solution via interaction between the quaternary ammonium and crown ether subunits. Steady-state fluorescence was used to determine the *K* value for the dyad system. The Benesi–Hildebrand method was applied to the data to determine a binding constant of about $375{,}000\ M^{-1}$ for the system. This value is two orders of magnitude higher than those of most coordinating systems previously studied. This very strong binding was rationalized by the presence of π–π stacking interactions between the porphyrin and C_{60} units, in addition to hydrogen bonding. Evidence for π–π stacking was provided by a ^{1}H NMR experiment where, upon addition of the C_{60} derivative to the crown ether appended porphyrin, the β-pyrrole protons of the porphyrin ring experienced an upfield shift. These data indicate that the porphyrin ring must be interacting with the C_{60} spheroid. Also, steady-state fluorescence experiments indicate that the presence of the C_{60} quaternary ammonium derivative quenches the singlet excited state of the porphyrin crown ether moiety efficiently.

Guldi et al. [122] prepared and studied self-assembled supramolecular dyad and triad systems composed of one or two phthalocyanine units (ZnPc or ZnPc–ZnPc) appended with a dibenzo-24-crown-8 unit capable of hydrogen bonding with a C_{60} molecule appended with a tertiary ammonium group (C_{60}amm) (Fig. 28b). Steady-state fluorescence data were used to obtain the *K* values for the studied systems. These values were determined to be $1.4 \times 10^4\ M^{-1}$ for the dyad system (ZnPc–C_{60}amm) and $1.9 \times 10^4\ M^{-1}$ for the triad system (ZnPc–C_{60}amm–ZnPc).

Time-resolved fluorescence experiments were employed to determine the nature of the excited state photochemical reactions for the dyad and triad systems. The two pristine ZnPc derivatives exhibited an excited state lifetime of around 3.1 ns. Upon addition of C_{60}amm, a short-lived component with a lifetime of 0.28 ns became predominant, accompanied by depletion of the long-lived component. The fast decay of the excited state of ^{1}ZnPc* upon complexation with C_{60}amm suggests that intramolecular ET from ^{1}ZnPc* is the predominant quenching mechanism.

Transient absorption spectral studies were performed to determine the nature of the species produced during the

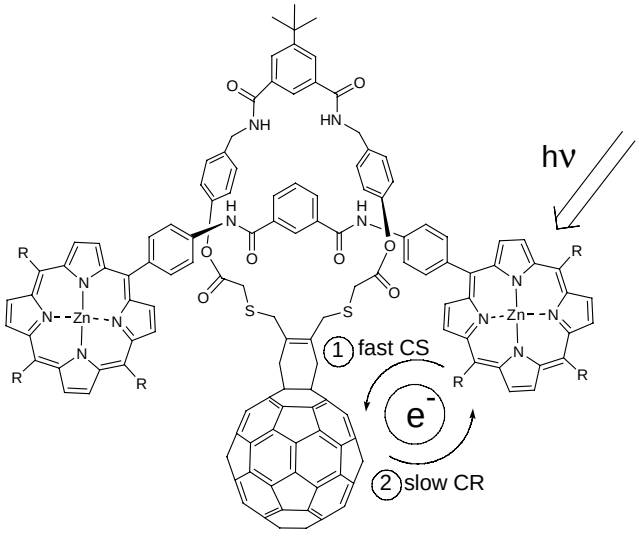

Fig. 29. Structure of the bis zinc porphyrin–fullerene rotaxane supramolecule.

course of the excited state photochemical reaction. Upon excitation with a 8 ns laser light flash, after 50 ns, bands at 1040 nm corresponding to $C_{60}amm^{\bullet -}$ and bands at 500 and 860 nm corresponding to $ZnPc^{\bullet +}$ were observed. These data indicate that the formation of SSIP occurs with a high Φ_{cs} value of about 0.90 and a lifetime (τ_{cs}) of 1.5 μs.

Recently, Watanabe et al. [123] reported intrarotaxane electron transfer between ZnTPP and C_{60}-crown ether in a supramolecular system shown in Fig. 29. The time profile of the fluorescence decay of the rotaxane revealed a biexponential decay in BN. From this data, efficient CS ($k_{cs} = 10^{10}\,s^{-1}$) from ^{1}ZnTPP* to the fullerene entity was calculated. The evaluated rate of CR from nanosecond transient absorption spectral studies by monitoring the decay of $C_{60}^{\bullet -}$ was found to be $5.5 \times 10^6\,s^{-1}$. This value corresponded to a lifetime τ_{RIP} of 180 ns for the CS state (radical ion pair). The observed slow CR suggested that this process was located in the Marcus-inverted region far more negative than the CS process.

4. Summary

The intermolecular ET processes from electron donors (porphyrins, chlorophyll, phthalocyanines, and naphthalocyanines) and their metal derivatives to electron acceptors, fullerenes (C_{60}/C_{70}) studied by nanosecond and picosecond laser flash photolysis techniques in polar and nonpolar solvents have revealed many interesting features. In polar solvents, the ET process takes place via the triplet excited states of the excited acceptor or excited donor, yielding solvated radical ion pairs. Because of the bimolecular encounter of solvated radical ion pairs, the back ET rates are found to be generally slow. The structure-photochemical reactivity probed in the intermolecularly interacting systems revealed dependence on the nature of the porphyrin/phthalocyanine macrocycle, the metal ion present in the porphyrin/phthalocyanine cavity, electron donor substituents on the macrocycle periphery, and the polarity of the solvent medium.

The porphyrins, phthalocyanines and fullerenes have been found to be excellent building blocks for supramolecular systems for the study of photoinduced CS reactions by using time-resolved ultrafast spectroscopic techniques. In the supramolecular conjugates formed by axial coordination, hydrogen bonding, crown-ether complexation, or rotaxane formation, the CS process occurs mainly from the singlet excited state of the donor. In contrast to the intermolecular back ET process, the back CR rates are found to be fast. In some of the conjugates studied, the predicted acceleration of the CS process and deceleration of the CR process have been clearly observed, mainly due to the small reorganization energies of fullerenes in electron transfer reactions. The photophysical properties of the porphyrin and fullerene moieties are shown to be tuned in a controlled manner upon coordination of metal centers. The nature of the linker between the donor and acceptor entities, the solvent, and the metal ions in the porphyrin cavity influences the overall photochemical reactivity. Studies on self-assembled supramolecular triads, tetrads, etc., are only in the beginning stages, and future studies will be anticipated to involve more complex systems targeted for better charge stabilization and also to perform specific light-driven photochemical processes. The supramolecular approach of building fullerene–porphyrin and fullerene–phthalocyanine conjugates is beginning to provide well-characterized donor–acceptor systems, which could eventually be used for the development of solar energy harvesting and opto-electronic devices such as sensors, switches, gates, etc.

Acknowledgements

The authors are thankful to the donors of the Petroleum Research Fund (administered by the American Chemical Society), the National Institutes of Health (to FD), the Japan Ministry of Education, Science, Technology, Culture and Sports, and the Mitsubishi Foundation (to OI and ME) for support of this research. ME is thankful to the Egypt Ministry of Scientific Research. PMS is thankful to the Department of Education for a GAANN fellowship.

References

[1] H.D. Roth, A brief history of photoinduced electron transfer and related reactions, in: J. Mattay (Ed.), Topics in Current Chemistry, vol. 156, Springer-Verlage, Berlin, 1990, pp. 1.
[2] J.S. Connolly, J.R. Bolton, in: M.A. Fox, M. Chanon (Eds.), Photoinduced Electron Transfer, Elsevier, Amsterdam, 1988.
[3] G.J. Kavarnos, N.G. Turro, Chem. Rev. 86 (1986) 401.
[4] M.R. Wasielewski, D.G. Johnson, W.A. Svec, K.M. Kersey, D.E. Cragg, D.W. Minsek, in: J.R. Norris, D. Meisel (Eds.), Photochemical Energy Conversion, Elsevier, Amsterdam, 1989.
[5] S. Mattes, S. Farid, Science 226 (1984) 917.
[6] D.F. Eaton, Electron transfer process in imaging, in: J. Mattay (Ed.), Topics in Current Chemistry, Springe-Verlage, Berlin, 1990, p. 199.
[7] M.R. Wasielewski, Chem. Rev. 92 (1992) 435.
[8] G.J. Kavarnos (Ed.), Fundamentals of Photoinduced Electron Transfer, VCH Publisher, New York, 1993, p. 103.
[9] D. Gust, T.A. Moore, A.L. Moore, in: Z.W. Tian, Y. Cao (Eds.), Photochemical and Photoelectrochemical Conversion and Storage of Solar Energy, International Academic Publishers, Beijing, 1993.
[10] C. Stegeman, P. Likamwa, in: A. Miller, K.R. Welford, B. Daino (Eds.), Nonlinear Optical Materials and Devices for Applications in Information Technology, Kluwer Academic Publishers, Amsteradm, 1995.
[11] J. Deisenhofer, in: J.R. Norris (Ed.), The Photosynthetic Reaction Center, Academic Press, San Diego, 1993.
[12] R.E. Blankenship, M.T. Madigan, C.E. Bauer (Eds.), Anoxygenic Photosynthetic Bacteria, Kluwer Academic Publishers, Dordrecht, 1995.
[13] D. Gust, T.A. Moore, A.L. Moore, in: F.S. Sterrett (Ed.), Alternative Fuels and the Environment, Lewis Publishers, Chelsea, 1995.
[14] J.S. Connolly (Ed.), Photochemical Conversion and Storage of Solar Energy, Academic Press, New York, 1981.
[15] V. Balzani (Ed.), Electron Transfer in Chemistry, vol. I–V, Wiley-VCH, Weinheim, 2001.

[16] D. Rehm, A. Weller, Isr. J. Chem. 8 (1970) 259.
[17] A.Z. Weller, Phys. Chem. 132 (1982) 93.
[18] D. Gust, T.A. Moore, in: K.M. Kadish, K. Smith, R. Guilard (Eds.), The Porphyrin Handbook, vol. 8, Academic Press, San Diego, 2000, pp. 153–190.
[19] D. Gust, T.A. Moore, A.L. Moore, Acc. Chem. Res. 26 (1993) 198.
[20] K. Yoshihara, S. Kumazaki, J. Photochem. Photobiol. C: Rev. 1 (2000) 22.
[21] I. Okura (Ed.), Photosensitization of Porphryins and Phthalocyanines, Gordon and Breach Science Publishers, Amsteradm, 2001.
[22] Y. Amao, I. Okura, J. Mol. Catal. B: Enzym. 17 (2002) 9.
[23] Y. Amao, K. Asai, T. Miyashita, I. Okura, Polym. Adv. Technol. 11 (2000) 705.
[24] K. Maruyama, A. Osuka, N. Mataga, Pure Appl. Chem. 66 (1994) 867.
[25] A. Osuka, N. Mataga, T. Okada, Pure Appl. Chem. 69 (1997) 797.
[26] H.Z. Staab, R. Hauck, B. Popp, Eur. J. Org. Chem. (1998) 631.
[27] T. Häberle, J. Hirsch, F. Pöllinger, H. Heitele, M.E. Michel-Beyerle, C. Ander, A. Döhling, C. Krieger, A. Rückemann, H.A. Staab, J. Phys. Chem. 100 (1996) 18269.
[28] K. Kilsa, J. Kajanus, A.N. Macpherson, J. Martensson, B. Albinsson, J. Am. Chem. Soc. 123 (2001) 3069.
[29] O. Korth, A. Wiehe, H. Kurreck, B. Roder, Chem. Phys. 246 (1999) 363.
[30] D.A. Williamson, B.E. Bowler, Inorg. Chim. Acta 297 (2000) 47.
[31] Y.-P. Sing, W. Huang, R. Guduru, R.B. Martin, Chem. Phys. Lett. 353 (2002) 353.
[32] C.S. Foote, in: K. Prassides (Ed.), Physics and Chemistry of the Fullerenes, Kluwer Academic Publishers, Amsteradm, 1994, p. 79.
[33] D.M. Guldi, P.V. Kamat, in: K.M. Kadish, R.S. Ruoff, (Eds.), Fullerenes, Chemistry, Physics and Technology, Wiley-Interscience, New York, 2000, p. 225.
[34] S. Nath, H. Pal, A.V. Sapre, Chem. Phys. Lett. 360 (2002) 422.
[35] F. Diederich, C. Thilgen, Science 271 (1996) 317.
[36] H. Imahori, Y. Sakata, Adv. Mater. 9 (1997) 537.
[37] A. Hirsch (Ed.), The Chemistry of the Fullerenes, Georg Thieme, Stuttgart, 1994.
[38] Q. Xie, E. Perez-Cordero, L. Echegoyen, J. Am. Chem. Soc. 114 (1992) 3978.
[39] J.-F. Nierengarten, J.-F. Eckert, D. Felder, J.-F. Nicoud, N. Armaroli, G. Marconi, V. Vicinelli, C. Boudon, J.-P. Gisselbrecht, M. Gross, G. Hadziioannou, V. Krasilkov, L. Ouali, L. Echegoyen, S.-G. Liu, Carbon 38 (2000) 1587.
[40] P.M. Allemand, A. Koch, F. Wudl, Y. Rubin, F. Diederich, M.M. Alvarez, S.J. Anz, R.L. Whetten, J. Am. Chem. Soc. 113 (1991) 1050.
[41] D. Dubois, K.M. Kadish, S. Flanagan, R.E. Haufler, L.P.F. Chibante, L.J. Wilson, J. Am. Chem. Soc. 114 (1992) 4364.
[42] A. Watanabe, O. Ito, H. Saito, M. Watanabe, M. Koishi, J. Chem. Soc., Chem. Commun. (1996) 117.
[43] D.M. Guldi, C. Luo, M. Prato, A. Troisi, F. Zerbetto, M. Scheloske, E. Dietel, W. Bauer, A. Hirsch, J. Am. Chem. Soc. 123 (2001) 9166.
[44] C. Luo, M. Fujitsuka, A. Watanabe, O. Ito, L. Gan, Y. Huang, C.-H. Huang, J. Chem. Soc., Faraday Trans. 94 (4) (1998) 527.
[45] M.M. Alam, A. Watanabe, O. Ito, Bull. Chem. Soc. Jpn. 70 (8) (1997) 1833.
[46] A. Watanabe, O. Ito, J. Phys. Chem. 98 (1994) 7736.
[47] O. Ito, Y. Sasaki, Y. Yoshikawa, A. Watanabe, J. Phys. Chem. 99 (1995) 9838.
[48] H. Imahori, Y. Mori, J. Matano, J. Photochem. Photobiol C: Photochem. Rev. 4 (2003) 51.
[49] D.M. Guldi, Chem. Soc. Rev. 31 (2002) 22.
[50] S. Fukuzumi, H. Imahori, H. Yamada, M.E. El-Khouly, M. Fujitsuka, O. Ito, D.M. Guldi, J. Am. Chem. Soc. 123 (2001) 2571.
[51] S. Fukuzumi, H. Imahori, K. Okamoto, H. Yamada, M. Fujitsuka, O. Ito, D.M. Guldi, J. Phys. Chem. A 106 (2002) 1903.
[52] K. Ohkubo, H. Imahori, J. Shao, Z. Ou, K.M. Kadish, Y. Chen, G. Zheng, R.K. Pandey, M. Fujitsuka, O. Ito, S. Fukuzumi, J. Phys. Chem. A 106 (2002) 10991.
[53] K.M. Smith (Ed.), Porphyrins and Metalloporphyrins, Elsevier, Amsterdam, 1975.
[54] S. Takagi, H. Inoue, in: V. Ramamurthy, K.S. Schanze (Eds.), Multimetallic and Macromolecular Inorganic Photochemistrt, Marcel Dekker, New York, 1999, pp. 215–342.
[55] S.A. Azim, M.A. El-Kemary, S.A. El-Daly, H.A. El-Daly, M.E. El-Khouly, Z.M. Ebeid, J. Chem. Soc., Faraday Trans. 92 (1996) 747.
[56] J.W. Owens, R. Smith, R. Robinson, M. Robins, Inorg. Chim. Acta 279 (1998) 226.
[57] A. Tsuda, A. Osuka, Science 93 (2001) 79.
[58] J.-H. Chou, M.E. Kosal, H.S. Nalwa, N.A. Rakow, K.S. Suslick, in: K.M. Kadish, K.M. Smith, R. Guilard (Eds.), The Porphyrin Handbook, vol. 6, Academic Press, New York, 2000.
[59] C. Lee, D.H. Lee, J-I. Hong, Tetrahedron Lett. 42 (2001) 8665.
[60] N.R. Armstrong, J. Porphyrins Phthalocyanines 4 (2000) 414.
[61] A. Blank, T. Galili, H. Levanon, J. Porphyrins Phthalocyanines 5 (2001) 58.
[62] K.C. Hwang, D. Mauzerall, J. Am. Chem. Soc. 114 (1992) 9705.
[63] K.C. Hwang, D. Mauzerall, Nature 361 (1993) 138.
[64] M.E. Milanesio, M. Gervaldo, L.A. Otero, L. Sereno, J.J. Silber, E.N. Durantin, J. Phys. Org. Chem. 15 (2002) 844.
[65] D.M. Guldi, P. Neta, K.-D. Asmus, J. Phys. Chem. 98 (1994) 4617.
[66] Y. Fujisawa, O. Yasunori, S. Yamauchi, Chem. Phys. Lett. 282 (1998) 181.
[67] Y. Fujisawa, O. Yasunori, S. Yamauchi, Chem. Phys. Lett. 294 (1998) 248.
[68] D.M. Martino, H. van Willigen, J. Phys. Chem. A 104 (2000) 10701.
[69] T. Nojiri, A. Watanabe, O. Ito, J. Phys. Chem. A 102 (1998) 5215.
[70] M.E. El-Khouly, M. Fujitsuka, O. Ito, J. Porphyrins Phthalocyanines 4 (2000) 591.
[71] T. Nojiri, M.M. Alam, H. Konami, A. Watanabe, O. Ito, J. Phys. Chem. A 101 (1997) 7943.
[72] T. Da Ros, M. Prato, D.M. Guldi, E. Alessio, M. Ruzzi, L. Pasimeni, Chem. Commun. (1999) 635.
[73] T. Da Ros, M. Prato, D.M. Guldi, M. Ruzzi, L. Pasimeni, Chem. Eur. J. 7 (2001) 816.
[74] D.M. Guldi, C. Luo, T. Da Ros, M. Prato, E. Dietel, A. Hirsch, Chem. Commun. (2000) 375.
[75] D.M. Guldi, C. Luo, A. Swartz, M. Scheloske, A. Hirsch, Chem. Commun. (2001) 1066.
[76] F. Diederich, M.G. Lopez, Chem. Soc. Rev. 28 (1999) 263.
[77] P. Piotrowiak, Chem. Soc. Rev. 28 (1999) 143.
[78] F. D'Souza, G.D. Deviprasad, M.E. El-Khouly, M. Fujitsuka, O. Ito, J. Am. Chem. Soc. 123 (2001) 5277.
[79] F. D'Souza, G.R. Deviprasad, M.E. Zandler, V.T. Hoang, K. Arkady, M. van Stipdonk, A. Perera, M.E. El-Khouly, M. Fujitsuka, O. Ito, J. Phys. Chem. A 106 (2002) 3243.
[80] F. D'Souza, G.R. Deviprasad, M.E. Zandler, M.E. El-Khouly, M. Fujitsuka, O. Ito, J. Phys. Chem. B 106 (2002) 4952.
[81] G. Yin, D. Xu, Z. Xu, Chem. Phys. Lett. 365 (2002) 232.
[82] J.R. Weinkauf, S.W. Cooper, A. Schweiger, C.C. Wamser, J. Phys. Chem. A 107 (2003) 3486.
[83] A. Bettelheim, D. Ozer, R. Harth, J. Electroanal. Chem. 226 (1989) 93.
[84] N. Gunduz, T. Gunduz, M. Hayvali, Talanta 48 (1999) 71.
[85] D. Wrobel, J. Lukasiewicz, J. Goc, A. Waszkowiak, R. Ion, J. Mol. Struct. 555 (2000) 407.
[86] M. Gouterman, in: D. Dolphin (Ed.), Porphyrins, vol. III, Academic Press, New York, 1978.
[87] A. Ramsdell, C.C. Wamser, J. Phys. Chem. 96 (1992) 10572.
[88] C.-l. Lin, M.-Y. Fang, S.-H. Cheng, J. Electro. Chem. 531 (2002) 155.

[89] S.I. Murov, Handbook of Photochemistry, Marcel Dekker, New York, 1985.
[90] K. Kalyanasundaram, Photochemistry of Polypyridine and Porphyrin Complexes, Academic Press, London 1992.
[91] C.A. Steren, H. von Willigen, L. Biczok, N. Gupta, H. Linschitz, J. Phys. Chem. 100 (1996) 8920.
[92] M.M. Alam, A. Watanabe, O. Ito, J. Photochem. Photobiol. A: Chem. 104 (1997) 59.
[93] M.E. El-Khouly, M. Fujitsuka, O. Ito, Phys. Chem. Chem. Phys. 4 (2002) 3322.
[94] J.K. Roy, F.A. Cattol, D.G. Whitten, J. Am. Chem. Soc. 96 (1974) 6349.
[95] M.E. El-Khouly, Y. Araki, M. Fujitsuka, O. Ito, Photochem. Photobiol. 74 (2001) 22.
[96] A.J. Hoff, J. Amesz, in: H. Scheer (Ed.), Chlorophylls, CRC Press, Boca Raton, 1992, p. 723.
[97] H. Scheer, in: W.M. Horspool, P.-S. Song (Eds.), Organic Photochemistry and Photobiology, CRC Press, Boca Raton, 1995, p. 1402.
[98] M. Guergous-Kuras, B. Boudreaux, A. Joliet, P. Joliot, K. Redding, Biophysics 98 (2001) 4437.
[99] B. Hales, J.R. Bolton, J. Am. Chem. Soc. 49 (1972) 3314.
[100] S. Itoh, M. Iwaki, I. Ikegami, Bioenergetics 1507 (2001) 115.
[101] M.E. El-Khouly, S.D.-M. Islam, M. Fujitsuka, O. Ito, J. Porphyrins Phthalocyanines 4 (2000) 713.
[102] F.H. Moser, A.L. Thomas, The Phthalocyanines, CRC Press, Boca Raton, FL, 1983.
[103] C.C. Lenzoff, A.Z.P. Lever (Eds.), Phthalocyanines, Properties and Applications, VCH Publishers Inc., New York, 1989.
[104] K.-Y. Law, Chem. Rev. 93 (1993) 449.
[105] S. Komel, B.J. Tromberg, W.G. Robeters, M.W. Bern, Photochem. Photobiol. 50 (1989) 175.
[106] Y. Shirota, J. Mater. Chem. 10 (2000) 1.
[107] G.A. Kumar, J. Thomas, N.V. Unnikrishnan, V.P.N. Nampoori, C.P.G. Vallabhan, J. Porphyrins Phthalocyanines 5 (2001) 456.
[108] N. Kobayashi, Coord. Chem. Rev. 227 (2002) 129.
[109] M. Antonietta Loi, P. Denk, H. Hoppe, H. Neugebauer, C. Winder, D. Meissner, C. Brabes, N.S. Sariciftci, A. Gouloumis, P. Vzquez, T. Torres, J. Mater. Chem. 13 (2003) 700.
[110] J. Morenzin, C. Sclebusch, B. Kessler, W. Eberhardt, Phys. Chem. Chem. Phys. 1 (1999) 1765.
[111] K.C. Hwang, D. Mauzerall, J. Am. Chem. Soc. 114 (1992) 9705.
[112] H. Luo, M. Fujitsuka, O. Ito, M. Kimura, J. Photochem. Photobiol. A: Chem. 156 (2003) 31.
[113] M.E. El-Khouly, L.M. Rogers, M.E. Zandler, S. Gadde, M. Fujitsuka, O. Ito, F. D'Souza, Chem. Phys. Chem. 4 (2003) 474.
[114] F. D'Souza, G.R. Deviprasad, M.S. Rahman, J.-P. Choi, Inorg. Chem. 38 (1999) 2157.
[115] N. Armaroli, F. Diederich, L. Echegoyen, T. Habicher, L. Flamigni, G. Marconi, J.-F. Nierengarten, New J. Chem. (1999) 77.
[116] F. D'Souza, N.P. Rath, G.R. Deviprasad, M.E. Zandler, Chem. Commun. (2001) 267.
[117] S.R. Wilson, S. MacMahon, F.T. Tat, P.D. Jarowski, D.I. Schuster, Chem. Commun. (2003) 226.
[118] F. D'Souza, G.R. Deviprasad, M.E. Zandler, M.E. El-Khouly, M. Fujitsuka, O. Ito, J. Phys. Chem. A 107 (2003) 4801.
[119] F. D'Souza, G.D. Deviprasad, M.E. El-Khouly, M. Fujitsuka, O. Ito, J. Am. Chem. Soc. 123 (2001) 5277.
[120] M.E. El-Khouly, S. Gadde, G.R. Deviprasad, M. Fujitsuka, O. Ito, J. Porphyrins Phthalocyanines 7 (2003) 1.
[121] N. Solladié, M.E. Walther, M. Gross, T.M.F. Duarte, C. Bourgogne, J.-F. Nierengarten, Chem. Commun. (2003) 2412.
[122] D.M. Guldi, J. Ramey, M.V. Martinez-Diaz, A. de la Escosura, T. Torres, T. Da Ros, M. Prato, Chem. Commun. (2002) 2774.
[123] N. Watanabe, N. Kihara, Y. Furusho, T. Takata, Y. Araki, O. Ito, Angew. Chem., Int. Ed. 42 (2003) 681.

Mohamed E. El-Khouly was born in Egypt in 1969. Mohamed graduated from the Chemistry Department, Tanta University, Egypt in 1991. He received his MS in 1996, under the guidance of Professor El-Zeiny M. Ebeid. In 1998, he joined the group of Professor Osamu Ito (Tohoku University, Japan) where he received his PhD in 2002. There he conducted research aimed at studying the electron transfer process of porphyrin–fullerene systems. After that, he returned to Egypt where he was promoted to the lecturer degree at Tanta University. Recently, he conducted postdoctoral studies in Professor Akihide Kitamura's Laboratory at Chiba University, Japan. His research interests involve photophysical and photochemical behavior of porphyrin compounds, Inter- and intra-molecular electron transfer process of porphyrin–fullerene systems by means of laser flash photolysis techniques.

Osamu Ito was born in 1943 in Ibaraki, Japan. He completed his PhD from Department of Chemistry, Graduate School of Science, Tohoku University in 1973; doctor thesis was about the circular dichroism of radical ion of biaryls. He became research associate of Research Institute of Nonaqueous Solution Chemistry of Tohoku University, where he found a selective scavenging flash photolysis technique to reveal the reversible free radical reactions. Then, he became associate professor of Institute for Chemical Reaction Science of Tohoku University and he is presently a professor of Institute of Multidisciplinary Research for Advanced Materials of Tohoku University. His main areas of research are photochemistry mechanism using of laser techniques in the wide wavelength and wide time regions. Main target is electron transfer processes of highly conjugated materials such as fullerene derivatives, porphyrins/phthalocyanines, oligothiophenes, etc. He was given the 39th Mitsubishi Foundation Award in 2002.

Phillip M. Smith was born in Wichita, Kansas, USA in 1976. He received BS degree from the Wichita State University in 2000 and is currently a graduate research assistant working towards a PhD degree under the supervision of Prof. Francis D'Souza. His research is focused on the synthesis and physico-chemical characterization of porphyrin and fullerene containing molecular and supramolecular systems for the study of photoinduced electron and energy transfer, and electrochemical applications.

Francis D'Souza was born in Sagar, Karnataka, India. He received BSc and MSc degrees from the Mysore University, Mysore, India and a PhD degree in 1992 from the Indian Institute of Science, Bangalore, India, under the direction of Prof. V. Krishnan. Following postdoctoral fellowships with Prof. Karl M. Kadish at the University of Houston, Texas and Prof. Roger Guilard at Université de Bourgogne, Dijon, France, he joined the Faculty of Wichita State University in 1994 and became a professor in 2003. His research interests are mainly focused on the synthesis, electrochemical, bioanalytical, and photochemical applications of porphyrin and fullerene supramolecular systems.